universität wien

MASTERARBEIT / MASTER'S THESIS

Titel der Masterarbeit / Title of the Master's Thesis

„LDL/HDL Distribution and Surface Properties in Water Slab“

verfasst von / submitted by

Alexander Gorfer, BSc

angestrebter akademischer Grad / in partial fulfilment of the requirements for the degree of

Master of Science (MSc)

Wien, 2020 / Vienna, 2020

Studienkennzahl lt. Studienblatt / degree programme code as it appears on the student record sheet:	UA 066 876
Studienrichtung lt. Studienblatt / degree programme as it appears on the student record sheet:	Masterstudium Physik
Betreut von / Supervisor:	Univ.-Prof. Mag. Dr. Christoph Dellago

Acknowledgement

Right from starting my work on this thesis up to the present moment, I received a great deal of support from multiple people.

I want to express my gratitude to my supervisor Prof. Christoph Dellago. His door was always open, and the thesis would not have been possible without his insightful feedback. The same is true for the supervision I received from Dr. habil. Marcello Sega and I want to dearly thank both for their patient support and guidance throughout every step of the way.

I would like to acknowledge the staff at the Sensengasse 8 for their warm welcome, their words of encouragement and for their helpful insights in furthering my research.

I would like to thank all the professors, researchers and friends I had the privilege to meet during my time at the University of Vienna, the University of Graz and Graz University of Technology. At the latter I would like to especially thank Dr. Markus Holzmann, who guided me during my bachelor's thesis, sharpened my thinking and pushed my work to higher levels.

In addition, I would like to thank my family for providing me with unfailing support throughout my academic life. I greatly attribute my interest in the natural sciences to my late father and – even though water is the natural enemy of the architect – I believe he would have enjoyed this work. This thesis is dedicated to his memory.

Abstract

Water behaves in unusual ways as it is supercooled. The divergence of thermodynamic response functions has led to a hypothesized liquid-liquid transition (LLT) in an experimentally inaccessible region of temperature that has in turn motivated two-structure theories of water describing it as a mixture of two competing structures; low-density liquid (LDL) and high-density liquid (HDL). Simultaneously, controversy exists if the surface tension of supercooled water follows the extrapolation of the IAPWS-equation or if it goes through a second inflection point (SIP) and exponentially rises above expected values. Both controversies and recent findings of a compact water layer, called the apophysis, beneath the surface of supercooled water make the vapour-liquid system an interesting object for exploratory research. In this thesis, extensive MD-simulations of an interfacial system of TIP4P2005 water were conducted from 198.15 to 348.15 K. The resulting surface tension shows an anomalous rise that would suggest an SIP. Two methods locate its temperature at about 278 K, which coincides with the density anomaly of TIP4P2005 but is 20 K higher than prior investigations. Using the ITIM algorithm to identify the first four interfacial layers, the apophysis was established to occur from the first layer getting more compact. Novel interfacial features of supercooled water such as an anomalous high HDL-fraction in the second layer were detected and connected to the apophysis. In connecting the SIP to the LLT, fluctuations of surface tension and HDL-fraction imply HDL-fraction to be negatively correlated with surface tension, which opens up questions that may help in unifying the SIP and the apophysis with the LLT.

Zusammenfassung

Die Eigenschaften von Wasser verändern sich in abnormaler Art und Weise im unterkühlten Bereich. Die starke Zunahme der thermodynamischen Antwortfunktionen hat zur Hypothese der „liquid-liquid-transition“ (LLT) geführt, die sich in experimentell unzugänglich tiefen Temperaturen befinden könnte. Daraus motivierte Theorien beschreiben Wasser als eine Mischung zweier konkurrierender Strukturen; „low-density liquid“ (LDL) und „high-density liquid“ (HDL). Gleichzeitig wird diskutiert ob die Oberflächenspannung von unterkühltem Wasser der Extrapolation der IAPWS-Gleichung genügt, oder ob sie einen zweiten Wendepunkt (SIP) beschreibt und exponentiell über die zu erwarteten Werte steigt. Diese beiden möglichen Anomalien sowie neuerliche Erkenntnisse einer kompakten Wasserschicht unterhalb der Oberfläche von unterkühltem Wasser, die sogenannte Apophysis, motivieren eine gründliche Erkundung solch eines Systems. In dieser Masterarbeit wurden ausführliche MD-Simulationen eines Dampf-Wassersystems von 198.15 bis 348.15 K mit dem TIP4P2005 Wassermodell durchgeführt. Die berechnete Oberflächenspannung zeigt ein anormales Wachstum, das mit dem SIP übereinstimmen würde. Zwei Methoden lokalisieren ihn bei ungefähr 278 K, was mit dem beobachteten Dichtemaximum von TIP4P2005 übereinstimmen würde, aber 20 K höher als eine frühere Studie ist. Mit dem ITIM-Algorithmus wurden die ersten vier Molekülschichten der Oberfläche bestimmt und die Apophysis mit der Kompaktifizierung der obersten dieser Schichten identifiziert. Neue Eigenschaften der unterkühlten Wasseroberfläche wie eine anormal hohe Konzentration von HDL in der zweiten Schicht wurden entdeckt und mit der Apophysis in Verbindung gebracht. Es wurde eine negative Korrelation zwischen Oberflächenspannung und HDL-Struktur beobachtet. Dies erschließt neue Forschungsfragen, die helfen könnten, sowohl den SIP als auch die Apophysis mit der LLT zu begründen.

Contents

Acronyms

AMBER	Assisted Model Building with Energy Refinement
CHARMM	Chemistry at HARvard Molecular Mechanics
GROMACS	GROningen MAchine for Chemical Simulations
GROMOS	GROningen MOlecular Simulation
HDA	High Density Amorphous ice
HDL	High Density Liquid
IAPWS	the International Association for the Properties of Water and Steam
ITIM	Identification of Truly Interfacial Molecules
LDA	Low Density Amorphous ice
LDL	Low Density Liquid
LLT	Liquid Liquid Transition
MC	Monte Carlo
MD	Molecular Dynamics
SIP	Second Inflection Point
SPC/E	Simple Point Charge/Extended
ST2	– a water model proposed by Stillinger and Rahman
TIP4P	Transferable Intermolecular Potential with 4 Points
TSEOS	Two Structure Equation Of State
VHDA	Very High Density Amorphous ice

Das Wasser ist ein freundliches Element für den,
der damit bekannt ist und es zu behandeln weiß.

Goethe, *Die Wahlverwandtschaften*

Introduction

Water is an omnipresent substance on earth and beyond that plays an essential role in almost all aspects of our life. Its anomalous chemical and physical properties, many of which are crucial for life as we know it, have been the topic of study since antiquity. A central theme in today's research are the properties of supercooled water. This metastable liquid state naturally occurs in different types of cloud formations such as cirrus and orographic wave clouds or continental convective storms in which water droplets can even reach temperatures of down to −38 °C [1]. The properties of water in its supercooled state are highly relevant in different fields, such as climatology [2] or cryobiology [3].

One of the greatest challenges faced in studying supercooled water is simply its tendency to spontaneously freeze before a proper measurement can be taken. The process of freezing instantly advances after an ice nucleus of critical size has formed, which restricts possible observations of supercooled water into a time window below the rate of nucleus formation. At temperatures deeper than the homogenous ice nucleation temperature T_H of about −38 °C this nucleation rate becomes shorter than currently accessible experimental timescales and most measurements are impossible. The region below T_H has thus been coined the *no-man's land* and due to it being experimentally inaccessible, the properties of water in and at its vicinity are topics of intense debate.

One of these is the question of what lies behind the drastic changes in waters thermodynamic response functions like its heat capacity, isobaric compressibility or its coefficient of thermic expansion inside the supercooled regime. A popular proposal hypothesizes a liquid-liquid-transition (LLT) in supercooled water [4]. This is a first order transition between two structurally distinct liquid phases of water; an icelike low density liquid (LDL) and an unstructured high density liquid (HDL). The origin of the divergent behaviour of the thermodynamic response functions could be attributed to the critical point of this phase transition inside the no-man's land.

A second topic is the debated second inflection point (SIP) of water's surface tension. Above the melting point, the surface tension of water agrees with an equation of the International Association for the Properties of Water and Steam (IAPWS). But there is controversy if it continues to follow an extrapolation of this equation in the supercooled regime, or if it goes through an inflection and exponentially rises above expected values. Recent experiments at extreme supercooling [5] have shown a deviation from the IAPWS-equation below −20 °C that leave open the possibility of an SIP. The surface tension of deeply supercooled water is important to model droplet formation and aerosol-liquid interaction which in turn are essential in describing cloud processes [6].

Due to the no-man's land, both the LLT-proposal and the SIP continue to evade experimental verification. However, the emergence of computer simulations has proven

itself in providing an additional route to generate insights into these topics. Direct methods such as molecular dynamics (MD) simulations work on much shorter timescales than the nucleation rate, allowing us to probe supercooled, albeit virtual, water inside experimentally inaccessible regions.

The search for an LLT in computational models of water has seen a great interest in the last decade. Previous research strongly suggest an LLT in the water models of ST2 [7, 8, 9] and TIP4P2005 [10, 11] as well as other models reviewed in [4]. In addition to suggesting an LLT, Singh et al. [10] have also used HDL and LDL in a binary mixture model to develop a two-structure equation of state (TSEOS) for TIP4P2005.

Also the possibility for an SIP has been researched using computer simulations. To calculate the surface tension with a water model one can use MD-simulations on systems containing both vapour and liquid water, separated by an interface. This method has been used to highly suggest an SIP in SPC/E [12, 13] and show support of an SIP in WAIL [14] and TIP4P2005 [13]. Apart from the SIP, there have also been multiple intriguing reports of a compact water layer (called the *apophysis*) immediately below the interface of supercooled water [15, 16, 17, 18, 19, 13].

This thesis set out to examine both the surface tension of a water model and the structural properties, particularly the distribution of LDL and HDL at the interface for a wide range of temperatures, including deeply in the supercooled regime. The TIP4P2005, likely exhibiting an LLT and properly conforming to a TSEOS of LDL and HDL with support of an SIP and the intriguing apophysis was chosen as our specimen. Using extensive MD-simulations we have investigated the interfacial profile from the viewpoint of a binary mixture of HDL and LDL and re-examined the purposed SIP of this model. In our structural analysis we have made use of the algorithm; Identification of Truly Interfacial Molecules (ITIM) to examine the structure of the first four interfacial layers and determined that the apophysis originates from a compactification of layer I. Drawing upon multiple strands of research, we attempt to shed light on the SIP from the standpoint of water as a binary mixture and concurrently illuminate both the SIP, the apophysis and the structure of HDL/LDL inside the interfacial system.

The thesis is composed into 6 chapters and a conclusion. The first two chapters present respectively the background behind current research into the LLT and the SIP. The third chapter reviews the theory required to conduct and analyse MD-simulations of interfacial systems. In the fourth chapter, suitable water models will be discussed. The subsequent chapter will give a detailed account on the simulation and introduce several advanced methods of analysis. Finally, in the sixth chapter the results are presented and discussed, before we give some concluding remarks, including an outlook toward future investigations.

1 Water and its Anomalies

In the following pages we will be presenting general properties of water, including the anomalies of its thermodynamic response functions and the multiple forms of ice in its phase diagram. We will then take a close look at the properties of supercooled water and make note of the multiple forms of metastable glass phases before discussing the hypothesis of the liquid-liquid-transition (LLT).

1.1 General properties

The water molecule consists of two hydrogen atoms covalently bound to one oxygen atom. In the equilibrium state these three nuclei lie at the corners of an isosceles triangle. The legs of this triangle are the O − H bonds with a length of $r_{\mathrm{OH}} = 0.96\,\text{Å}$ and its vertex angle $\angle_{HOH}$ is 104.5°. An excitation leads to an increase in both bond length and vertex angle [20]. Water does not have a molecular center of symmetry and the geometric arrangement of its partial charges results in a relatively strong permanent electric dipole moment of 1.84 Debye [20].

An essential characteristic of water is its inclination to form hydrogen bonds. In total, a water molecule consists of ten electrons. Two of those are associated with the oxygen atom and the other eight hybridize into the four tetrahedral sp^3 molecular orbitals. Two of these molecular orbitals make up the two covalent O − H bonds. The other two *lone-pair* orbitals are situated outside the molecular plane to form the sp^3-shape [21].

A hydrogen bond between two water molecules is an intermolecular bond between a lone-pair orbital of the acceptor and a hydrogen atom of the donor [21]. They have a strength of about $20\,\mathrm{kJ\,mol^{-1}}$ [22] and are highly directional, in the sense that they are maximized when the hydrogen atom and both respective oxygen atoms of donor and acceptor are collinear [23]. The strength might be small compared to that of a covalent bond of approximately $400\,\mathrm{kJ\,mol^{-1}}$ but is much larger than the strength of pure London dispersive interaction, which is on the order of $1\,\mathrm{kJ\,mol^{-1}}$ [22].

The hexagonal structure of ordinary ice ($\mathrm{I_h}$) is succinctly described as an ordered hydrogen bonded network. Every water molecule in $\mathrm{I_h}$ accepts two hydrogen atoms of different water molecules and donates its hydrogen atoms to yet two others. This leads to a network of oxygen atoms that are separated by hydrogen atoms and coordinated in the direction of the vertices of a regular tetrahedron [22]. The distance between neighbouring oxygen atoms in this arrangement is 2.74 Å [22], making the lattice less dense than liquid water, which results in $\mathrm{I_h}$ floating on liquid water.

Apart from $\mathrm{I_h}$ we know of 16 additional solid crystalline phases that appear at high pressures and various temperatures. In Fig. 1.1 (and the review of Brini et al. [21] in particular) some are illustrated.

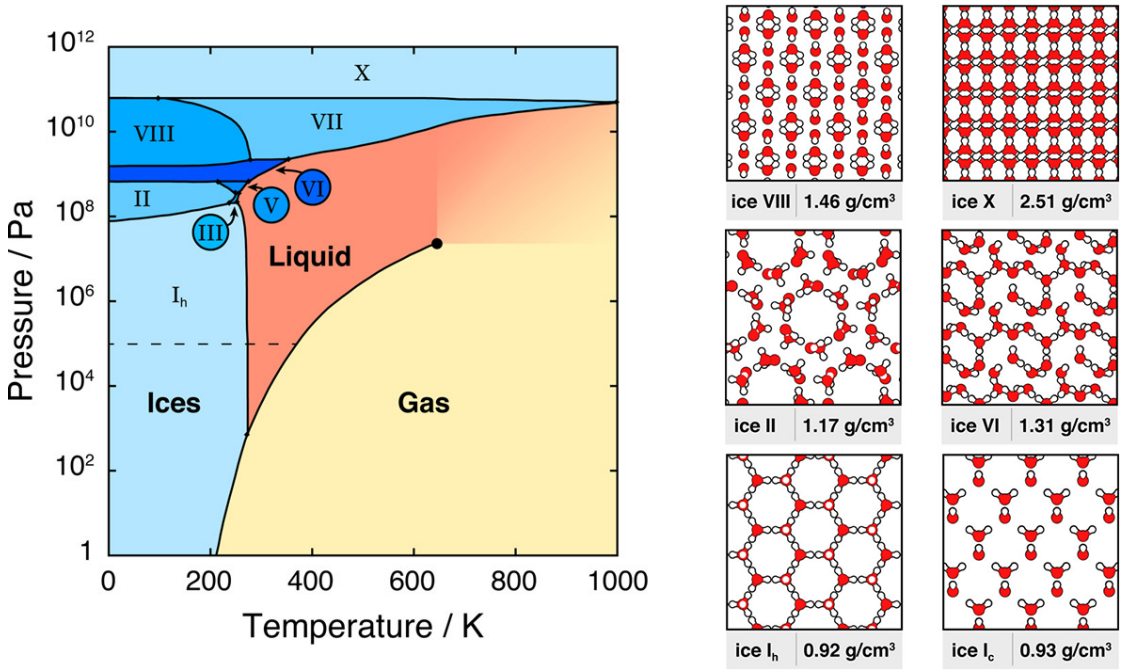

Figure 1.1: Representative phase diagram of water. The proton-ordered phases are not shown. A visualization of different ice phases and their respective density is included on the right. Higher pressures correlate with denser phases. In ice X hydrogen bonds and covalent bonds even become undistinguishable as the hydrogen atoms are shared equally between oxygen atoms. Both images reprinted from Brini et al. [21] under the terms set in *ACS AuthorChoice*.

The ability to hydrogen-bond is not a unique feature of the crystalline phase. Even though there is no long-range crystalline structure in liquid water, its molecules will still have a tendency to form hydrogen bonds. To solidify liquid water at atmospheric pressures the necessary heat of fusion is only $6\,\mathrm{kJ\,mol^{-1}}$ [22], considerably less than the necessary energy to form hydrogen bonds. Since I_h is a fully hydrogen bonded network, the implication is that some hydrogen bonding must persist in liquid water.

The strength and persistence of hydrogen bonds make water an unusually cohesive substance. Furthermore, the fact that the energetic preference for tetrahedral bonding persists in liquid water results in the rare case of it having a negative correlation between energy and volume, and between entropy and volume at low temperatures [22].

Some further anomalous behaviours are illustrated in Fig. 1.2. Apart from the well-known density maximum at about 4 °C, water also has an unusually small coefficient of thermal expansion α_T [24] that drastically decreases with temperature and even becomes negative below the density maximum. Notable is also that the isothermal compressibility κ_T goes through a minimum at 319 K, after which water becomes more compressible the deeper it is cooled. A similar minimum is visible in the isobaric heat capacity C_P of water at 311 K for 0.1 MPa [24]. Of particular interest is that the anomalous change in

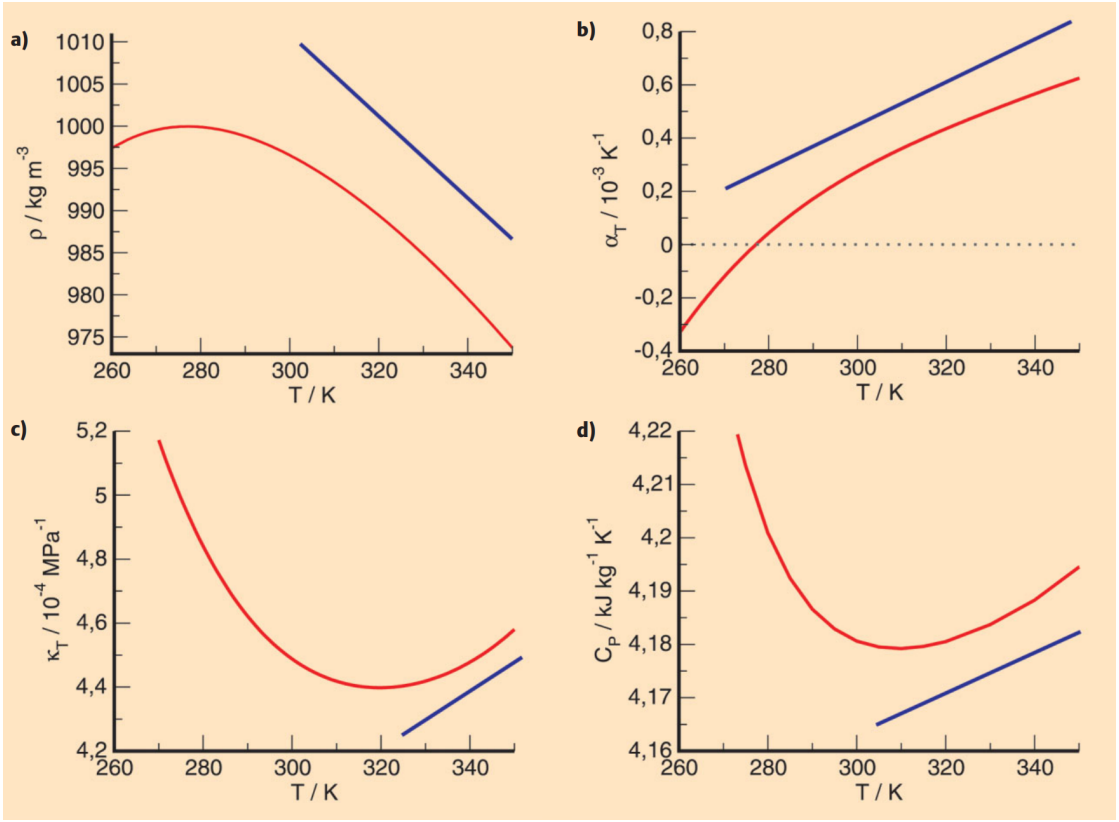

Figure 1.2: Some thermodynamical anomalies of water (red) versus a simple liquid (blue). Pictured in; **a)** is the density anomaly, **b)** is the coefficient of thermal expansion, **c)** is the isothermal compressibility and **d)** is the isobaric heat capacity at 0.1 MPa. Notice how the divergences get ever more exacerbated towards deep levels of supercooling. Image reprinted from Ludwig and Paschek [24].

these thermodynamic response functions intensifies the deeper water is supercooled.

1.2 Supercooled water and nucleation rates

The melting point T_{M} of a substance is the pressure-dependent temperature above which the liquid state will be the thermodynamically stable phase and below which the solid state will be thermodynamically stable. All liquids can however to some degree be cooled below T_{M} without them crystallizing. They are in a metastable supercooled liquid phase and will not solidify until a seed crystal or nucleus of the solid phase has formed at nucleation-inducing impurities or through stochastic motion. After a nucleus has formed the barrier toward solidification is gone and the phase transformation proceeds rapidly.

Reaching moderate temperatures of supercooling can be accomplished with tap water

and a domestic freezer. By a similar but more dangerous token, one can also (unwillingly) create superheated water with highly impure watery solutions such as coffee or tea inside a domestic microwave. Once an ice crystal or a bubble appears in these metastable states the transition toward ice and respectively steam occurs explosively.

But to achieve more extreme temperatures while remaining liquid, a low concentration of nucleation-inducing impurities and the absence of vibrations and irregularities in the container is required. The further water is cooled away from its stable state, the more difficult this becomes and may require elaborate methods such as purifying water droplets to averagely contain less than one impurity [25] and then suspending them to keep them out of contact with container walls [26].

The solidification depends on the formation of nuclei of critical size. Once such an ice nucleus has formed in supercooled water, the molecules in its vicinity will crystallize on its surface and the ice nucleus thus grows via self-assembly until the substance has transitioned completely. This restricts possible observations of supercooled water into a time window below the rate of nucleus formation.

At most temperatures, the dominant process of nucleation is heterogenous nucleation, in which nuclei form at irregular sites such as impurities or rough container walls that guide the kinetics of the system to the appearance of the stable phase. However, the absence of irregularities does not prevent the phase transformation altogether. A different mechanism is homogenous nucleation, where the stochastic motion of molecules themselves leads to the creation of a nucleus of critical size [26].

In water the rate of homogenous nucleation starkly increases the further it is cooled below T_M, insofar as presenting an almost insurmountable challenge in regard to doing measurements on supercooled water at extremely low temperatures. Unlike heterogenous nucleation, homogenous nucleation cannot be prevented by keeping impurities and container walls away from the sample. The temperature at which the rate of homogenous nucleation rises above the timescales necessary for an observation of thermodynamic response functions such as heat capacity, isobaric compressibility or its coefficient of thermal expansion is called the homogenous nucleation temperature T_H which lies at about 235 K. This temperature is one border of a region in the p-T-diagram that is not accessible by most experiments called the *no-man's land*. The nucleation rate also depends on sample size and the necessary observation time, thus T_H is not a hard limit and researchers have managed to observe water on millisecond timescales at 227 K [23]. The rate of homogenous nucleation reaches a maximum deep in the no-man's land, after which it actually decreases with cooling, implying the possibility for ultraviscous supercooled water to be observable somewhere between the lower border of the no-man's land and above the glass transition temperature T_g. A temperature dependent classification of stability of liquid water is illustrated in Fig. 1.3.

1.3 Polyamorphism

Any liquid can be converted into a glass by cooling it quicker than the time to form a crystalline phase. To vitrify water in particular, rapid cooling on the order of around

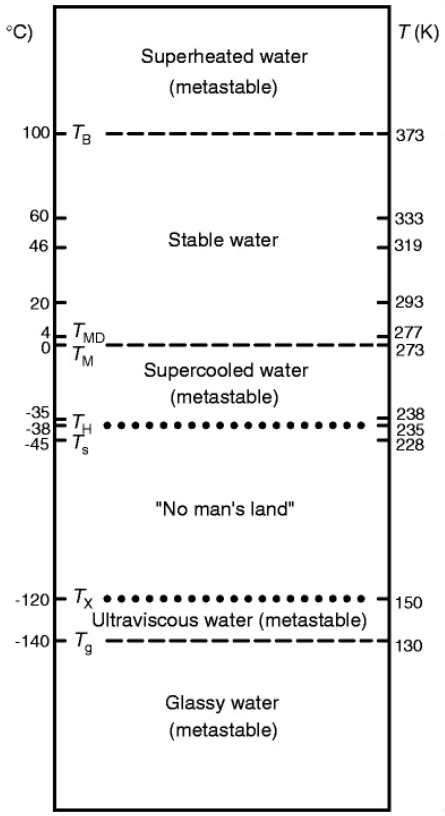

Figure 1.3: Phase classification of liquid water at atmospheric pressure. While only being stable between 0 °C and 100 °C, liquid water can continue to exist in metastable states in extreme conditions. Image adapted from Mishima and Stanley [27].

10^6 K s^{-1} [22, 28] below the glass transition temperature T_g of about 136 K is necessary. Below T_g, the liquid structure is arrested and the substance becomes the amorphous solid that is a glass (see for example [26]). Like supercooled water, the amorphous phase of water is metastable in regard to a crystalline phase and when it is heated up to the temperature of spontaneous crystallization T_X, it crystallizes. Thus, T_X marks the lower border of the no-man's land. Whereas these temperatures are not found on earth, glassy water might actually be the most prevalent form of water in the universe, populating interstellar dust clouds and comets [29].

In addition to the multiple solid crystalline phases pictured in Fig. 1.1, it is also a peculiarity of water that one is able to distinguish between multiple solid amorphous phases. Handle et al. [23] define these as distinct nonaging and noncrystallizing amorphous structures and identify at least three such phases in water. The difference in the microscopic arrangement of these glasses gives them different densities, thus they are aptly named; low- (LDA), high- (HDA), and very-high-density-amorphous ice (VHDA).

In LDA the water molecules have four neighbours in the first coordination shell in a

structure reminiscent of the hexagonal I_h network but without long-range order [23]. In HDA the tetragonal arrangement is disturbed by additional molecules encroaching into the first shell. The number of besiegers rises with pressure, going from 1 additional molecule at ambient pressure to 9 at 2 GPa [23]. In VHDA there are yet more molecules stepping into the first shell. At ambient pressures there are two additional neighbours in the first shell but with higher pressures the structural difference between HDA and VHDA diminishes [23].

1.4 The LLT proposal

A liquid-liquid-transition (LLT) is a first order phase transition between two different liquid phases. They commonly emerge in the form of a separation of chemical components in a liquid mixture but can also exist in monomolecular substances like liquid crystals or even between superfluid and normal phases in quantum liquids [4]. The LLT of water, in its current form proposed in 1992 [30], would be of a special density driven kind. It would be a separation of liquid phases with identical composition but different density [4]. Classical thermodynamics allow for such a phase transformation to happen and while still unusual, experiments have suggested its occurrence in some materials [31, 32].

A primary point of consideration for an LLT in water is that it offers an appealing explanation for the puzzling divergent behaviour of the thermodynamic response function in supercooled water (illustrated in Fig. 1.2). LLTs are first order phase transitions and come with an associated critical point where thermodynamic and dynamical properties diverge (see for example [33]). A critical point below T_H would be in line with the divergent behaviour. In Fig. 1.4, a possible LLT with critical point and loci of maxima of thermodynamic responses is illustrated for the TIP4P2005 water model.

Furthermore, the LLT would offer a root cause for the multiple phases of amorphous ice. The LLT-proposal necessitates the occurrence of two distinct liquid phases of different density; low-density liquid (LDL) and high-density liquid (HDL). The vitrification of either might be respectively identified with LDA and HDA.

Additionally, starting with an attempt of Röntgen to describe the density maximum of water [37], theoretical approaches that model water as a mixture of two competing structures have seen a lot of development. Recent approaches in applying two-structure thermodynamics have resulted in equations of state that are in excellent agreement with the properties of supercooled water [38]. While the existence of two structures in water would not automatically imply a liquid-liquid critical point or even a liquid-liquid transition inside the no-man's land [39], two-structure thermodynamics does offer an appealing theoretical background to the LLT.

Due to the difficulty of crystallization in the no-man's land, direct observations of an LLT in real water have not been possible. There have however been a large number of classic studies that are in line with precursors or echoes of an LLT [40, 41, 42].

Computer simulations in particular have been extensively applied to explore the nature of an LLT. The current proposal of the LLT was even established by a study of ST2-water [30] and recent research also suggests an LLT in the TIP4P2005 water model [10].

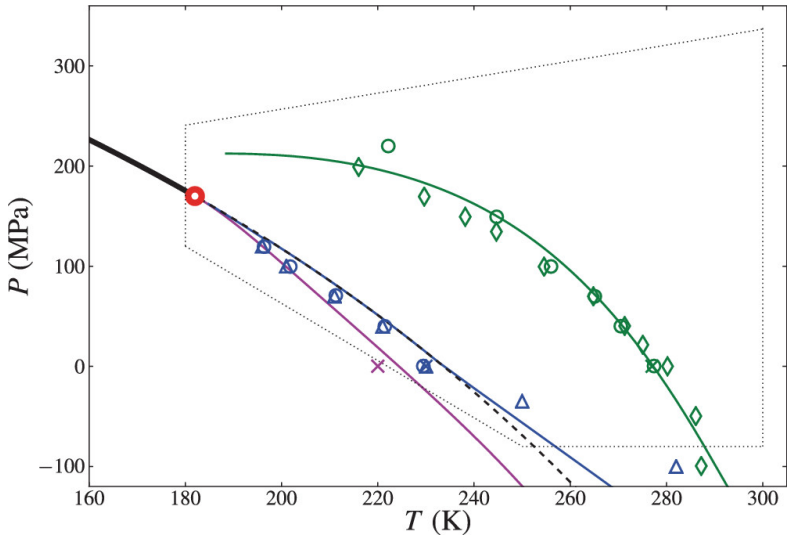

Figure 1.4: Possible phase diagram with an LLT of the TIP4P2005 water model, calculated from a TSEOS of Singh et al. [10] in the supercooled regime. The thick black line is the phase transition between LDL and HDL which ends in the liquid-liquid critical point (red circle). The dashed curve represents the Widom line of this transition. Illustrated are also the loci of maximal density ρ (green curve), of isothermal compressibility κ_T (blue curve) and isobaric heat capacity C_P (purple curve). Data of these maxima is shown from [34] (diamonds), [35] (circles), [36] (triangles) and [10] (crosses). The TSEOS of Singh et al. is valid inside the dotted region. Image reprinted from Singh et al. [10]. Copyright AIP publishing LLC.

2 Surface Tension

The tendency of liquids to minimize their surface area and form droplets is described by surface tension. It is a mesoscopic property that originates in the interaction between the microscopic liquid phase components. For the calculation and subsequent analysis of surface tension in this thesis we require two different viewpoints. A possible picture of surface tension is that of the number of broken bonds per unit area, leading to dimensions of energy per area. Equivalently we can also think about surface tension as a pulling force parallel to the surface of water, resulting in dimensions of force per length. In the sections that follow we will discuss both approaches before discussing the hypothesis of the second inflection point (SIP) of water's surface tension.

The molecular origin of surface tension can be traced to cohesive and repulsive forces between the liquid phase components. For a molecule in the bulk liquid there are on the average the same number of neighbouring molecules in any direction. This means that both the repulsive forces from very near neighbours as well as the attractive forces from neighbours farther away respectively average to zero. For molecules closer to the surface this is no longer the case. The surface cuts off the distribution of neighbours and - due to the cohesion of liquids - particles experience a net attractive force away from the surface. They accelerate inwards until they get too close to interior molecules where they are stopped by repulsive interactions and reach an equilibrium [43].

2.1 Thermodynamic approach

A molecule at the surface has fewer neighbours and therefore fewer intermolecular bonds than a molecule in the bulk. Thus, to increase a surface area Σ requires some intermolecular bonds to be broken so that bulk molecules can be converted to interfacial molecules. We denote the (reversible) work required for an infinitesimal increase of surface by [44]

$$\delta W = -\gamma \mathrm{d}\Sigma.$$

The MD-simulations of this thesis will be done in an ensemble of constant temperature T, volume V and particle number N. Consequently, we use the Helmholtz free energy F as our thermodynamic potential. By including δW in the respective differential form we obtain [44]:

$$\mathrm{d}F = -S\mathrm{d}T - P\mathrm{d}V + \gamma \mathrm{d}\Sigma, \tag{2.1}$$

from which immediately follows a defining equation of the surface tension:

$$\gamma = \left(\frac{\partial F}{\partial \Sigma}\right)_{T,V}. \tag{2.2}$$

From Eq. 2.1 we can also infer the Maxwell relation [44]:

$$\left(\frac{\partial\gamma}{\partial T}\right)_{V,\Sigma} = -\left(\frac{\partial S}{\partial \Sigma}\right)_{T,V}.$$

Integrating over $\mathrm{d}\Sigma$ results in an interfacial entropy term $S_S(T,\Sigma)$ and a bulk entropy term $S_B(T,V)$:

$$S(T,V,\Sigma) = S_S(T,\Sigma) + S_B(T,V) = -\left(\frac{\partial\gamma}{\partial T}\right)_{V,\Sigma}\Sigma + c(T,V),$$

where the bulk contribution is an unknown function $c(T,V)$. We can identify the interfacial parts and use the fact that surface tension is a function of only temperature to get [44]:

$$\frac{S_S}{\Sigma} = -\frac{\mathrm{d}\gamma}{\mathrm{d}T}. \tag{2.3}$$

This quantity is called the surface excess entropy per unit area and it usually decreases with temperature. In Chapter 6 we will record an anomalous rise in the surface excess entropy of water and draw conclusions regarding the SIP.

The molecular origin of surface tension as the number of broken bonds makes it possible to estimate it using the binding energy ϵ and cross section σ^2 of a substance. The surface tension should be on the order of magnitude of ϵ/σ^2 [45]. This has the effect that if we look at the surface tension of the first 10 primary monohydric alcohols at room temperature we will find that they all fall between 24 and $30\,\mathrm{mN\,m^{-1}}$, the values for methanol and decan-1-ol respectively [46]. Viscosity, in comparison to surface tension, is a property that increases much more dramatically with particle size. The viscosity of nonan-1-ol is 14 times that of methanol. Due to hydrogen bonds, water has a comparatively much larger surface tension of $72\,\mathrm{mN\,m^{-1}}$ [46] while still having a viscosity similar to methanol. An order of magnitude above water still is mercury with a surface tension of $487\,\mathrm{mN\,m^{-1}}$ [46].

2.2 Mechanical approach

Alongside the thermodynamic definition of surface tension given in Eq. 2.2 it is also possible to approach γ from a more mechanical perspective. Let there be a vapor-liquid system in a coordinate system x-y-z with an interface at z_0 and let the system be homogenous over the x-y planes for all z. Due to this homogeneity the pressure p is only a function of the coordinate normal to the interface, z. The surface of tension is given by the x-y plane at z_0.

Let there now be a strip of length l and unit width in some y-z plane passing through the interface. If there was no surface to pass, there would be a uniform pressure p_0 around the strip creating a stress $(-p_0 \times l)$ in the x direction of the strip. We define the surface tension as the difference between the actual stress Σ_x and the uniform pressure[47]:

$$\gamma = \Sigma_x + \int_{\text{all } z} p(z).$$

Since our strip is of unit width, we can identify the stress Σ_x with the integral over the negative normal atomic pressure $-\int P_{xx}(z)\mathrm{d}z$, where $P_{\alpha\beta}$ denotes the pressure tensor. We can likewise identify $p(z)$ with $P_{zz}(z)$. We therefore get:

$$\gamma = \int_{\text{all } z} \Big(- P_{xx}(z) + P_{zz}(z)\Big)\mathrm{d}z.$$

Due to the homogeneity inside the x-y plane we can equivalently write $P_T = \frac{1}{2}(P_{xx}(z) + P_{yy}(z))$ instead of P_{xx}. In the MD-simulation we will save the pressure tensor over the whole system and calculate an ensemble average. In regard to this application we can write an equivalent formulation:

$$\gamma = \frac{L_z}{n}\left[\langle P_{zz}\rangle - \frac{1}{2}(\langle P_{xx}\rangle + \langle P_{yy}\rangle)\right], \tag{2.4}$$

where L_z is the length of the whole system and n is the number of interfaces between the two phases. The equivalence between Eq. 2.2 and Eq. 2.4 was shown by Alejandre et al. [48]. This mechanical definition was also derived in a thermodynamic approach by Tolman [49].

2.3 The second inflection point of surface tension

Since the properties of water are of immense industrial and scientific importance, there exists a non-profit association called the International Association for the Properties of Water and Steam (IAPWS) that among other tasks reviews and administrates standard values of these properties. The equation of the temperature dependence of surface tension of the IAPWS is of the following form [50]:

$$\gamma = B \cdot \left(\frac{T_\mathrm{c} - T}{T_\mathrm{c}}\right)^{\mu} \cdot \left(1 + b \cdot \frac{T_\mathrm{c} - T}{T_\mathrm{c}}\right), \tag{2.5}$$

with the critical temperature $T_\mathrm{c} = 647.096\,\mathrm{K}$ and parameters $B = 235.8\,\mathrm{mN\,m^{-1}}$, $b = -0.625$ and $\mu = 1.256$. This equation is an empirical fit to experiments of Vargaftik et al. [51] which were done between 0.01 °C and 374 °C. The validity of Eq. 2.5 below 0 °C is at the core of the debate on the SIP.

The surface tension γ of water goes through an inflection at a temperature T_1 of around 525 K [44]. Below T_1, the surface tension follows a concave curve as it falls with rising temperature. Above T_1 it continues to fall with rising temperature but does so in a convex fashion. In the language of differential calculus, $\frac{\mathrm{d}^2\gamma}{\mathrm{d}T^2}$ goes from negative at $T < T_1$ to positive at $T > T_1$ which is a sufficient criterion for the existence of an inflection point at T_1. Since $\frac{\mathrm{d}\gamma}{\mathrm{d}T}$ does not vanish, T_1 is not a saddle point. A computational study (that included TIP4P2005) suggests that this anomaly originates in a breakdown of the hydrogen-bonding network at the surface of water [52].

The second inflection point (SIP) of water is a neither proven nor disproven supposed inflection of surface tension in the supercooled regime. In similarity to the first inflection

at T_1 the hypothesis is that at low temperatures the surface tension goes through an inflection and begins increasing substantially faster with decreasing temperature than predicted by extrapolating the IAPWS-equation into the supercooled regime. While the measurements of Vargaftik et al. [51] did not include data below 0 °C, the extrapolation of the IAPWS formulation is still used as the archetypical trend below 0 °C.

An early notice of a growing increase in surface tension were the 1951 experiments of Hacker [53]. The property was also recognized in experiments carried out in the 1990s [54, 55]. However, Hrubý, Vinš, Hykl et al. in the mid-2010s managed to make measurements as far down as 250 K [56, 57, 58] without finding anomalous behaviour. Contrary to these results, the same group managed to measure the surface tension of extremely supercooled water down to 241.7 K and recorded a considerable deviation below 253 K to the IAPWS equation which would again make possible a second inflection point in the surface tension of real supercooled water [5].

3 Molecular Dynamics

In this chapter we move to the computational aspects of studying an interfacial system of water. We will first introduce the field that is the computational study of liquid systems. Then we will advance from basic statistical mechanics to essential algorithms used in our molecular dynamics (MD)-simulation.

Solids can be roughly classified as having both short- and long-range order, and gases to have no order at all. Liquids fall between these two extremes, being ordered at short range but becoming disordered at long ranges. To quantify this notion, we introduce the pair correlation function $g(r)$ of a system of particles that is defined as the deviation of the number of particles at a distance r to a homogenous (ideal gas) distribution of particles:

$$g(r) = \frac{1}{2\pi r^2 \rho N} \left\langle \sum_{i<j} \delta(r - r_{ij}) \right\rangle, \tag{3.1}$$

where ρ is the average density, N is the particle number and r_{ij} is the distance between particles i and j. This function describes the average local density at a radius r around a reference particle of the system. It allows us to characterize the local structure, as illustrated in the comparison of $g(r)$ for solid, liquid and gaseous argon in Fig. 3.1.

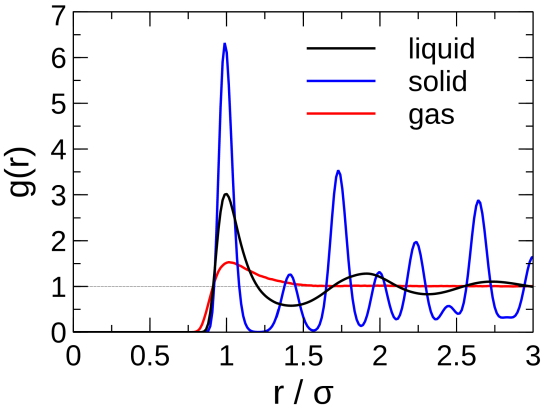

Figure 3.1: Pair correlation functions of solid (50 K), liquid (80 K) and gaseous (300 K) argon in reduced units of its molecular diameter σ. Whereas $g(r)$ stays sharply defined for the solid it immediately tends to the homogenous distribution ($g = 1$) for the gas. The liquid state is ordered on a short range and tends to the homogenous distribution further away. Image reprinted from *Wikimedia* [59] under the terms set in *CC BY-SA 4.0*.

The characteristic structure of liquids forbids the use of common simplifying assumptions

used for the other states of matter and narrows possible theoretical approaches. For liquids it may even prove challenging to begin formulating a reasonable approximation [60] and exactly solvable models are often highly idealized [61].

The understanding of the unique structure and particle dynamics found in liquids has greatly benefitted from the use of Monte Carlo (MC) and MD simulations. These methods need only the masses of atoms in a system and the interactions of these atoms in and between molecules (perhaps including multipoles) to calculate macroscopic properties such as pressure, temperature and surface tension.

Real liquids are made up of strongly interacting molecules. It would therefore seem necessary to evolve a liquid using the appropriate many-particle Hamiltonian. And while it is true that even macroscopic properties of condensed matter like pressure, temperature and volume can be thought of as resulting from interactions that can only be explained using quantum mechanics, the many-particle Hamiltonian is not something that is used directly in most cases. This is because firstly, the time dependent Schrödinger equation becomes too computationally demanding for systems made up of more than a few atoms, but also because it is often not necessary to know the microscopic interactions to make predictions of a macro- or even mesoscopic property.

3.1 Statistical mechanics

To describe this classical many-body system we can formulate a Lagrangian function $\mathcal{L}(\mathbf{q}, \dot{\mathbf{q}})$ where $\mathbf{q}$ are generalized coordinates and $\dot{\mathbf{q}}$ are their time derivatives. Let the Lagrangian be defined by some kinetic energy $\mathcal{K}$ and potential energy $\mathcal{V}$ in the following sense:

$$\mathcal{L} = \mathcal{K} - \mathcal{V}.$$

Consequently, the Lagrangian equation of motion holds:

$$\frac{\mathrm{d}}{\mathrm{d}t}(\partial\mathcal{L}/\partial\dot{\mathbf{q}}_k) - \partial\mathcal{L}/\partial\mathbf{q}_k = 0.$$

For a system of point masses this takes the form:

$$m_i\ddot{\mathbf{r}}_i = \mathbf{f}_i(\mathbf{r}^N), \tag{3.2}$$

where m_i is the mass, $\mathbf{r}_i$ the position and $\mathbf{f}_i$ the force acting on particle i. We can also formulate generalized momenta $\mathbf{p}_k = \frac{\partial\mathcal{L}}{\partial\dot{\mathbf{q}}_k}$ and write down the Hamiltonian

$$H(\mathbf{p}, \mathbf{q}) = \sum_k \dot{\mathbf{q}}_k\mathbf{p}_k - \mathcal{L}(\mathbf{q}, \dot{\mathbf{q}}), \tag{3.3}$$

with the Hamiltonian equations of motion in our case being:

$$\frac{\partial H}{\partial\mathbf{p}_k} = \dot{\mathbf{q}}_k = \mathbf{p}_i/m_i$$

$$\frac{\partial H}{\partial\mathbf{q}_k} = -\dot{\mathbf{p}}_k = \nabla_{\mathbf{r}_i}\mathcal{V} = -\mathbf{f}_i.$$

To evolve the system, we can either solve for the $3N$ coupled second order Lagrangian equations of motion or the $6N$ coupled first order Hamiltonian equations of motion. We choose the latter. Their solution is in the form of a trajectory $\mathbf{\Gamma}(t) = \left(\mathbf{r}^N(t), \mathbf{p}^N(t)\right)$ in the phase space of the system.

In a system without external forces the time derivate of the Hamiltonian vanishes, expressing the conservation of energy:

$$\frac{\mathrm{d}H}{\mathrm{d}t} = 0.$$

Also the total momentum is conserved and for an isolated set of particles also the total angular momentum. Together this reduces the size of the dynamical system to $6N - 6$ generalized coordinates.

Let $\mathbf{\Gamma} = \left(\mathbf{r}^N, \mathbf{p}^N\right)$ be a point in the phase space of this dynamical system. A solution has the form of a trajectory $\mathbf{\Gamma}(t)$ in phase space. Let $\mathcal{A}(\mathbf{\Gamma})$ be the instantaneous value of a macroscopic observable like temperature, pressure or volume at some point $\mathbf{\Gamma}$. We define the value of an observable over a trajectory $\mathbf{\Gamma}(t)$ as a time average:

$$\langle \mathcal{A} \rangle_{\text{time}} = \lim_{\tau \to \infty} \frac{1}{\tau} \int_0^\tau \mathrm{d}t \; \mathcal{A}(\mathbf{\Gamma}(t)), \tag{3.4}$$

where τ is the length of the available trajectory. If the system is ergodic, meaning it can reach all of the available phase space volume in a finite amount of time, the observed average $\langle \mathcal{A} \rangle_{\text{time}}$ equals the desired ensemble average $\langle \mathcal{A} \rangle$, defined with an ensemble-specific probability density $f(\mathbf{\Gamma})$:

$$\langle \mathcal{A} \rangle = \frac{\int \mathrm{d}\mathbf{\Gamma} \mathcal{A}(\mathbf{\Gamma}) f(\mathbf{\Gamma})}{\int \mathrm{d}\mathbf{\Gamma} f(\mathbf{\Gamma})}. \tag{3.5}$$

In MD-simulations we use the time average to determine observables. To equate this average with the general ensemble average we must make sure that the trajectory fulfils ergodicity and that we let our system evolve for long enough to actually sample enough of the ensemble. The fact that we want to sample supercooled water further complicates this, as we have to let the system evolve for long enough to generate meaningful microstates of the metastable phase but not so long as to crystallize into its stable state.

On a calculatory note, the use of Eq. 3.4 to determine macroscopic observables also necessitates defining instantaneous values of the observables. When doing simulations, it is important to distinguish between macroscopic observables like temperature, which are defined as averages over an ensemble and instantaneous values of the same from single microstates. A thermometer that would measure an instantaneous temperature, which is dependent on the fluctuations of the kinetic energy, would not be able to determine thermal equilibria between systems and under the zeroth law of thermodynamics lose its status as a thermometer. This does not mean that the concept of instantaneous observables is ill-defined. We can think about them as those values that average to macroscopic observables under Eq. 3.4. For our MD-simulation and its analysis we need to define instantaneous values of temperature and pressure.

3.2 Determining T and P

Our system is composed of a simulation box with a definite volume containing a known number of molecules. This makes it easy to determine $V(\mathbf{\Gamma})$ and $N(\mathbf{\Gamma})$, even if we were to allow these values to fluctuate to sample an isobaric or grand canonical ensemble. But determining an instantaneous temperature or pressure is less straightforward. First, we make use of the equipartition theorem:

$$\left\langle z_i \frac{\partial H}{\partial z_j} \right\rangle = k_\mathrm{B} T \delta_{ij}, \tag{3.6}$$

where z_i is either a generalized position or generalized momentum, i.e. a coordinate in phase space. One can now define instantaneous values of observables through the form of the Hamiltonian function. Under the assumption that the Potential $\mathcal{V}$ is independent of particle velocity or time Eq. 3.3 simply becomes:

$$H = \mathcal{K} + \mathcal{V}. \tag{3.7}$$

In the simple case of $\mathcal{K} = \sum_i^N |\mathbf{p}_i|^2 / 2m_i$ we can sum over all $3N$ momentum degrees of freedom such that [60, Eq. 2.53]:

$$\left\langle \sum_{i=0}^{N} \frac{|\mathbf{p}_i|^2}{m_i} \right\rangle = 2\langle \mathcal{K} \rangle = 3Nk_\mathrm{B}T. \tag{3.8}$$

Since $\mathcal{K}$ is defined for any microstate we can define an instantaneous temperature by letting go of the ensemble average [60, Eq. 2.54]:

$$\mathcal{T} = \frac{2\mathcal{K}}{3Nk_B} = \sum_{i=0}^{N} \frac{|\mathbf{p}_i|^2}{m_i}. \tag{3.9}$$

Similarly, in defining an instantaneous pressure we can again make use of Eq. 3.6 but this time using generalized positions, arriving at [60]:

$$-\left\langle \sum_{i=0}^{N} \mathbf{r}_i \cdot \nabla_{\mathbf{r}_i} \mathcal{V} \right\rangle = \left\langle \sum_{i=0}^{N} \mathbf{r}_i \cdot \mathbf{f}_i^{\mathrm{tot}} \right\rangle = 3Nk_\mathrm{B}T. \tag{3.10}$$

Writing the pressure gets us:

$$\begin{aligned} P &= -\left(\frac{\partial E}{\partial V}\right)_T \\ &= -\left(\frac{\partial \mathcal{K}}{\partial V}\right)_T - \left(\frac{\partial \mathcal{V}}{\partial V}\right)_T, \end{aligned} \tag{3.11}$$

where we have identified $E = H$ using assumption 3.7. With the kinetic energy as given in Eq. 3.8 we can take the derivative using the ideal gas law after applying an ensemble average:

$$P = \frac{Nk_\mathrm{B}T}{V} - \left\langle \frac{\partial \mathcal{V}}{\partial V} \right\rangle. \tag{3.12}$$

For further deriving the pressure care must be taken on the geometry and type of potential used in the simulation. For a pairwise potential and periodic boundary conditions the pressure can be written as [62]:

$$P = \frac{N k_{\mathrm{B}} T}{V} + \frac{1}{6V} \left\langle \sum_{i=0}^{N} \sum_{j \neq i}^{N} \mathbf{r}_{ij} \cdot \mathbf{f}_{ij} \right\rangle . \tag{3.13}$$

Now it is possible to determine an instantaneous value for the pressure by leaving out the ensemble average. One is also free to choose $\mathcal{T}$ instead of T in Eq. 3.13, the average will not change, but the fluctuations in pressure will be different [60].

It is also possible to derive Eq. 3.13 in tensorial form, resulting in the following equation for the pressure tensor [63, Eq. 5.25]:

$$\begin{aligned} P_{\alpha\beta} &= \frac{1}{V} \left(\sum_{i}^{N} m_i \mathbf{v}_i \otimes \mathbf{v}_i - \sum_{i<j} \mathbf{r}_{ij} \otimes \mathbf{F}_{ij} \right) \\ P &= \mathrm{trace}(P_{\alpha\beta})/3 \end{aligned} \tag{3.14}$$

3.3 Finite difference approach to integrate the equations of motion

An analytical solution of the $6N - 6$ ordinary differential equations is possible only for some special cases such as that of the free particle or the harmonic oscillator. Hence the use of numerical computer algorithms to integrate the equations of more complicated systems and generate an approximate trajectory.

The idea in the method of finite differences is to discretize the full trajectory into snapshots separated by a timestep Δt. A point in phase space $\mathbf{\Gamma}(t_0)$ contains the positions and momenta necessary to approximate the point $\mathbf{\Gamma}(t_0 + \Delta t)$ for some timestep Δt. Once we have the point at $t_0 + \Delta t$ we can integrate to generate the point $\mathbf{\Gamma}(t_0 + 2\Delta t)$ and so forth.

A smaller timestep will lead to a better approximation of the real trajectory, but also increase the required computational effort. In the case of a many-body dynamical system the approximated trajectory will virtually never follow the real trajectory forever. Rather we expect the computed microstates – even when only considering the physical limit on numerical precision – to diverge exponentially in phase space with some Lyapunov exponent.

While this does undermine the physical validity of the approximated trajectory, it does not prevent us from calculating macroscopic properties from the approximation. We average over all generated points in phase space, thus as long as the timestep Δt is small enough to generate a valid microstate $\mathbf{\Gamma}(t_0 + \Delta t)$ from $\mathbf{\Gamma}(t_0)$, we will be able identify macroscopic properties. An essential identifier of such a valid microstate is the conservation of energy and momentum, which we cannot allow to drift. Two algorithms that ensure this are Verlet integration and the leapfrog algorithm.

3.4 Verlet and leapfrog algorithm

One classic method of numerically integrating Newton's second law of motion $\mathbf{F} = \frac{\mathrm{d}\mathbf{p}}{\mathrm{d}t}$, is Verlet integration. We start the derivation of this method with the Taylor expansion of the positions $\mathbf{r}(t_0 + \Delta t)$ and $\mathbf{r}(t_0 - \Delta t)$ from a known position $\mathbf{r}(t_0)$.

$$\mathbf{r}(t_0 + \Delta t) = \mathbf{r}(t_0) + \mathbf{v}(t_0)\Delta t + \frac{\mathbf{F}(t_0)}{2}\Delta t^2 + \frac{\dddot{\mathbf{r}}}{3!}\Delta t^3 + \mathcal{O}(\Delta t^4)$$
$$\mathbf{r}(t_0 - \Delta t) = \mathbf{r}(t_0) - \mathbf{v}(t_0)\Delta t + \frac{\mathbf{F}(t_0)}{2}\Delta t^2 - \frac{\dddot{\mathbf{r}}}{3!}\Delta t^3 + \mathcal{O}(\Delta t^4).$$

Reordering the second equation for $\mathbf{v}(t_0)\Delta t$ yields:

$$\mathbf{v}(t_0)\Delta t = \mathbf{r}(t_0) - \mathbf{r}(t_0 - \Delta t) + \frac{\mathbf{F}(t_0)}{2}\Delta t^2 - \frac{\dddot{\mathbf{r}}}{3!}\Delta t^3 + \mathcal{O}(\Delta t^4).$$

Putting this in the first equation yields:

$$\mathbf{r}(t_0 + \Delta t) = 2\mathbf{r}(t_0) - \mathbf{r}(t_0 - \Delta t) + \mathbf{F}(t_0)\Delta t^2 + \mathcal{O}(\Delta t^4), \tag{3.15}$$

which already defines the algorithm. Since the third order terms cancel each other this algorithm is accurate to $\mathcal{O}(\Delta t^4)$. The Verlet algorithm does not require knowledge about the velocities, but they can be calculated using the mean value theorem:

$$\mathbf{v}(t) = \frac{\mathbf{r}(t_0 + \Delta t) - \mathbf{r}(t_0 - \Delta t)}{2\Delta t} + \mathcal{O}(\Delta t^2). \tag{3.16}$$

This results in a large uncertainty in velocity and it being a full timestep behind the current position. The leapfrog algorithm uses the same integration scheme, but achieves a smaller error in the velocities by first applying the mean value theorem on half timesteps:

$$\mathbf{v}\left(t_0 + \tfrac{1}{2}\Delta t\right) = \frac{\mathbf{r}(t_0 + \Delta t) - \mathbf{r}(t_0)}{\Delta t} + \mathcal{O}(\Delta t^2) \tag{3.17a}$$

$$\mathbf{v}\left(t_0 - \tfrac{1}{2}\Delta t\right) = \frac{\mathbf{r}(t_0) - \mathbf{r}(t_0 + \Delta t)}{\Delta t} + \mathcal{O}(\Delta t^2). \tag{3.17b}$$

From 3.17a we can also write the position as:

$$\mathbf{r}(t_0 + \Delta t) = \mathbf{r}(t_0) + \mathbf{v}\left(t_0 + \tfrac{1}{2}\Delta t\right)\Delta t + \mathcal{O}(\Delta t^3) \tag{3.18}$$

Finally, in 3.15 we can move one $\mathbf{r}(t_0)$ to the left and divide by Δt to get it in terms of the velocities 3.17a and 3.17b, resulting in:

$$\mathbf{v}\left(t_0 + \tfrac{1}{2}\Delta t\right) = \mathbf{v}\left(t_0 - \tfrac{1}{2}\Delta t\right) + \mathbf{F}(t_0)\Delta t + \mathcal{O}(\Delta t^3). \tag{3.19}$$

Equations 3.18 and 3.19 define the leap frog algorithm. The local truncation error in both velocity and position is $\mathcal{O}(\Delta t^3)$.

Using one of the algorithms above we can already evolve a simple system. A global flow scheme of the code, used in the GROMACS MD-suite in particular [64] but in great similarity to all MD-simulations is the following:

1. Initialization
   - read in starting conditions
   - initialize system
2. Main loop
   - compute forces on each particle
   - integrate equations of motion for Δt
   - update configuration
   - if needed: write configuration to disk
   - repeat for the required number of steps
3. write out results and final configuration

3.5 Nosé–Hoover thermostat

With algorithms that satisfy the conservation of energy and a simulation box of fixed size we can already evolve a system in the microcanonical/NVE ensemble. For the purpose of this thesis however, we want to sample from the canonical/NVT ensemble. To fix temperature instead of energy we can use the Nosé–Hoover thermostat. This algorithm introduces – or more accurately – mimics the effects of a thermal reservoir by altering the equations of motions to sample the canonical ensemble.

Nosé accomplished this by extending the system to include an additional degree of freedom which drives the dynamics [65]. A slight alteration of the equations of motion by Hoover [66] managed to remove time scaling, leading to the Nosé–Hoover thermostat with the following equations of motion [60, Eq. 3.64]:

$$\begin{aligned} \dot{\mathbf{r}} &= \mathbf{p}/m \\ \dot{\mathbf{p}} &= \mathbf{f} - (p_\eta/Q)\,\mathbf{p} \\ \dot{\eta} &= p_\eta/Q \\ \dot{p}_\eta &= \mathbf{p}\cdot\mathbf{p}/m - g k_\mathrm{B} T, \end{aligned} \tag{3.20}$$

where T is the temperature to be driven toward and g is the number of degrees of freedom. Whereas Q is a constant, $\dot{p}_\eta$ changes according to the difference between the target temperature and instantaneous temperature $\mathcal{T}$, defined in Eq. 3.9. If $\mathcal{T} \geq T$ this will drive p and therefore $\dot{\eta}$ to bigger values and vice versa. This in turn drives the velocity of the particles to a distribution where $\mathcal{T}$ agrees with T.

The Hamiltonian that follows from Eq. 3.20 is [60, Eq. 3.65]:

$$\mathcal{H} = \mathcal{K} + \mathcal{V} + \frac{p_\eta^2}{2Q} + g k_\mathrm{B} T \eta. \tag{3.21}$$

3.6 Periodic boundary conditions

If we calculate intermolecular forces using a long-range potential, we have to account for each interaction of the N particles with the $N-1$ other particles. With this approach the computational complexity of an MD-simulation scales like $\mathcal{O}(N^2)$. There are computational schemes like limiting interactions to particles that are close together and physical approximations that can reduce this computational cost to $\mathcal{O}(N)$, but this still usually leaves the applicability of MD-simulations to lie in a range of 10 to 10^4 molecules [60].

With such a low number of particles, the sampling of macroscopic properties needs special care to be taken. Macroscopic systems have particle numbers in the range of Avogadro's Constant N_A of about 6×10^{23}. If we simulate in a cube-shaped system with dimensions $a \times a \times a$ we can estimate the number of particles that are on the surface to be on the order of a^2 whereas the bulk particles will be proportional to a^3. Assuming a macroscopic system where each particle fills one unit of volume: $N = |N_\mathrm{A}| = |a^3|$. In such a system virtually no particles are on the surface. In contrast, if we decrease the number of particles to $N = 1000$ we find that 49 % lie on the surface. The local environment of these surface particles is not the same as those in the bulk and skews our sample.

To simulate bulk properties using fewer particles we can use periodic boundary conditions instead of hard walls. Instead of there being a repelling potential at the boundaries of the box, particles leaving the box enter it from the opposite site. In two dimensions one can imagine the particles to be confined to the surface of a torus. Equivalently we can think of our system being made up of a lattice of periodically repeated, identical, space-filling simulation boxes. Particles can travel and interact with each other without being influenced by a boundary. This makes every particle a part of the bulk and allows for a much more accessible simulation of bulk properties.

While solving the problem of boundaries, periodic boundary conditions do not lead to the thermodynamic limit of $\{N \to \infty, V \to \infty, \frac{N}{V} = \text{const.}\}$ and there are pitfalls due the combination of periodicity and finite size. The appearance of physical phenomena is restricted to those that have an associated wavelength smaller than the size of the periodic box. One such phenomenon is the correlation length that diverges as we approach a critical point, including the hypothesized liquid-liquid critical point. Also, the interaction of particles with their own images can lead to periodic artefacts and should not be allowed to happen. The interaction range is therefore restricted, adhering to the minimum-image convention.

3.7 Simulating a vapour-liquid interface

To calculate the surface tension of water we need to simulate it in the inhomogeneous system containing a liquid phase and a vapour phase. A popular method to create a gas-liquid interfacial system – used at least since 1976 [67] – is that of the slab geometry.

First, the liquid phase is equilibrated by itself in a cube-shaped system with periodic

boundary conditions. Then the faces normal to the z-axis of the cube are extended outwards, creating a cuboid cell containing a liquid state and a vacuum part in periodic boundary conditions. This system is then equilibrated once more before configurations are written to disk. If the equilibration does not destroy the interfaces, the system will consist of a vapour part and a liquid part which are separated by two interfaces normal to the z-axis. With periodic boundary conditions we achieve a system as illustrated in Fig. 3.2.

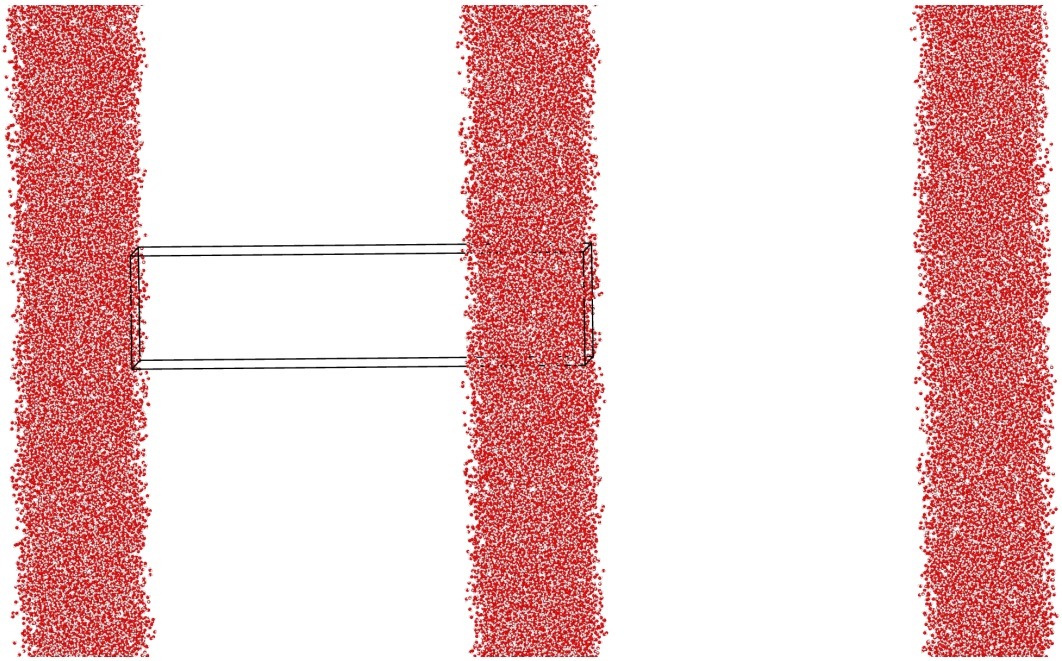

Figure 3.2: Snapshot of the slab geometry generated with TIP4P2005 water at 298.15 K. The black lines illustrate the borders of the simulation cell containing two vapour-liquid interfaces. Due to periodic boundary conditions the cell is infinitely repeated in all directions.

4 Water Modelling

Water was one of the earliest subjects of computer simulations and a multitude of models and simulation techniques have been applied to calculate its properties. Section 4.1 serves to account for a possible discrimination based on different length and timescales that are necessary to simulate different properties. Section 4.2 will focus on two rigid body models used in MD-simulations of the vapour-liquid interface.

4.1 Different approaches

At the smallest scale it is necessary to use explicit quantum mechanical techniques to solve the Schrödinger equation of 10 electrons per water molecule to gain an ab initio picture of bonds in and between water molecules. Simulating the full quantum mechanical nature quickly becomes too computationally expensive even for systems of only a few molecules [21].

An approximation to reach a higher number of water molecules is to use an ab initio force field for its quantum mechanical description and to employ fitting functions to approximate the polarizability of the oxygen atom. Structures with several hundred water molecules can be modelled this way [21].

To gain insight into processes at larger scales such as phase transformations or to model the structure of the bulk liquid state, classical intermolecular potentials between bodies of point masses and charges are used [21]. These can be rigid or flexible but mostly unpolarizable models that are developed semiempirically and try to balance the accuracy to experiment gained by additional parameters with the necessary computational effort.

Even coarser approaches are found in reducing the dimensionality of water to a sphere or even, in the case of the two-dimensional Mercedes-Benz model [68], to a circle with three arms for hydrogen bonding.

4.2 Rigid body models

Let us focus on the semiempirical models of point masses and charges that can be evolved using classical mechanics. We furthermore restrict ourselves to rigid bodies, in which the intramolecular bonds of the molecule are modelled using holonomic constraints as opposed to flexible bodies with spring interactions. With such constraints there are no bond oscillations, which are usually of high frequency and low amplitude, and a much greater timestep is possible. Since all but a few bonds inside a real substance are in their vibrational ground state, rigid bodies can be considered physically faithful [69].

One of the earliest simulations of molecular liquids – showing the feasibility of this approach to simulate water – was the 1969 MC-simulation of Barker and Watts [70]. A following influential work was the 1971 MD study by Rahman and Stillinger [71]. They used a tetragonal arrangement of four point charges around a Lennard-Jones site as their model and laid the foundation for the development of the prominent ST2 model over the course of the 1970s.

The 1980s saw the development of computationally more efficient models [21] such as the simple point charge (SPC) model of Berendsen [72, 73] and the transferable intermolecular potential (TIP) models of Jorgensen [74, 75].

The TIP models illustrate an important characterization of classical water models by their number of interaction sites. The straightforward approach of modelling the positions of the three constituent nuclei as charged point masses results in 3 interaction sites but additional *dummy* sites can be used to better approximate the charge distribution of the sp^3 molecular orbitals. Initially available as TIP3P (3 point) and TIP4P (4 point) the TIP family of models now also include TIP5P [76] and even TIP7P [77], published in the years 2000 and 2019 respectively.

The TIP3P model is a popular model due to its comparatively low required computational effort combined with good accuracy and used as the default water model in the standard force field of MD-engines like AMBER and CHARMM [21]. The SPC models, also 3-point, are used in the GROMOS engine and force field.

Let us now consider two water models in more detail; the extended simple point charge (SPC/E) model [78] and the TIP4P2005 model [79]. Their classic intermolecular interaction is done through two potentials; a Lennard-Jones term acting between the oxygen atoms:

$$u_{LJ}(r_{\mathrm{OO}}) = 4\epsilon \left[\left(\frac{\sigma}{r_{\mathrm{OO}}} \right)^{12} - \left(\frac{\sigma}{r_{\mathrm{OO}}} \right)^{6} \right], \tag{4.1}$$

where r_{OO} is the distance between the oxygen atoms and σ and ϵ are respectively the size and strength of the Lennard-Jones interaction. And an electrostatic potential between multiple charge sites:

$$u_{\mathrm{electrostatic}} = \frac{e^2}{4\pi\epsilon_0} \sum_{i \neq j} \frac{q_i q_j}{r_{ij}}, \tag{4.2}$$

where q_i, q_j are the partial charges and r_{ij} is the distance between the partial charges.

4.2.1 SPC/E

In 1987 Berendsen et al. published the SPC/E model [78] as a reparameterization in the charge distribution of the SPC model. It has three rigid interaction sites forming an isosceles triangle with a vertex angle $\angle_{\mathrm{HOH}}$ of 109.47°. This is the angle of the ideal tetrahedron and about 5° greater than the actual $\angle_{\mathrm{HOH}}$ found in water. In the SPC/E model all partial charges are situated at the nuclei. It is pictured in Fig. 4.1a and its complete parametrization is given in Table 4.1.

The SPC/E model was the first model that exhibits the general features of the water-ice phase diagram and also produces reasonable values of most other properties of water

[80]. For these reasons it might be the most widely studied model of water with a wealth of data for comparison. The melting point of SPC/E is at 213 K [81].

The SPC/E model exhibits some anomalous behaviour in line with an LLT [82], with one study of the potential energy landscape suggesting that a liquid-liquid critical point would be around the position of the glass transition, inhibiting the observation by slow glassy relaxation [83]. Furthermore, two studies suggest an SIP in SPC/E [12, 13].

4.2.2 TIP4P2005

The TIP4P2005 model of Abascal and Vega [79] is a reparameterization of Jorgensen's TIP4P model. There is a massless dummy particle that holds the negative partial charge of the oxygen atom. The bond lengths r_{OH} and the angle $\angle_{HOH}$ take on their experimental values. It is pictured in Fig. 4.1b and its complete parametrization is given in Table 4.1.

It can recreate the phase diagram of water with a high degree of accuracy, including the numerous crystalline phases therein [10].

The melting point of TIP4P2005 is at 249 K [81]. The density maximum is very close to real water and occurs at about 278 K for a pressure of 1 bar. The values of thermodynamic responses of the coefficient of thermal expansion α_T, the isothermal compressibility κ_T and the isobaric heat capacity C_P are closer to experiment than in TIP4P, TIP5P or TIP4P/EW [79].

In TIP4P2005 there are multiple studies suggesting the existence of an LLT. One using the potential energy landscape [11] and multiple using MD [34, 35, 84, 10]. Furthermore, two-state equations of state accurately predict thermodynamic properties of TIP4P2005 [85, 10] (see also Fig. 1.4). The existence of an SIP around 240 - 250 K was also recently suggested [13].

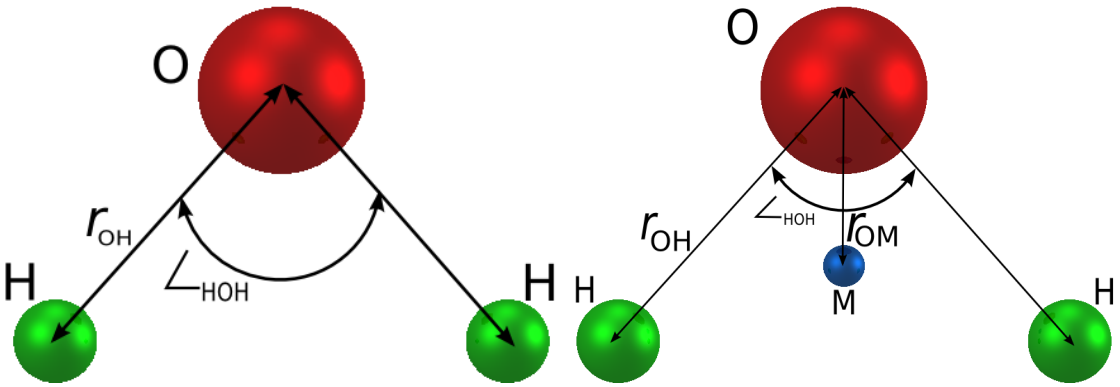

(a) Three site model (b) Four site model

Figure 4.1: Water models with three or four interaction sites typically take the form above. Particularly SPC/E and TIP4P2005. Images reprinted from Sklogwiki [86] under the terms set in *CC BY-NC-SA 3.0*.

Table 4.1: Details on the parameters used in the SPC/E [78] and TIP4P2005 [79] models pictured in Fig. 4.1. In both models the partial charges cancel each other to result in a net charge of zero. The coefficients σ and ϵ are respectively the size and strength of the Lennard-Jones center on the oxygen atom.

Parameters	SPC/E	TIP4P2005
σ	3.166 Å	3.1589 Å
ϵ	0.650 kJ mol^{-1}	0.7749 kJ mol^{-1}
r_{OH}	1.000 Å	0.9572 Å
r_{OM}	-	0.1546 Å
$\angle_{\mathrm{HOH}}$	109.47°	104.52°
q_{O}	$-0.8476\,e$	$0.0000\,e$
q_{H}	$-1/2 \times q_{\mathrm{O}}$	$0.5564\,e$
q_{M}	-	$-2 \times q_{\mathrm{H}}$

5 Methods

The following pages describe the process of simulating the interfacial system as well as giving a more detailed account in the methods that were applied to explore for an SIP, for the apophysis and for determining the HDL/LDL distribution over the interfacial system.

5.1 Molecular dynamics simulation

We oriented ourselves on the existing set of simulations of Wang, Binder, Chen et al. [13] for the water models SPC/E (Section 4.2.1) and TIP4P2005 (Section 4.2.2). In their study, SPC/E was simulated in steps of 10 K from 198.15 K up to 348.15 K and TIP4P2005 in steps of 10 K from 218.15 K up to 348.15 K. In our study we focused on TIP4P2005, repeating the simulations of Wang et al. for TIP4P2005 and expanding the range to include 5 additional temperatures in areas of interest given in Table 5.1. These MD-simulations were done with the GROMACS 2019.3 [87] MD-suite.

Motivated by the description of creating a slab-geometry given in Section 3.7 and in close similarity to Wang et al. [13], we initialized a cubic system measuring $5 \times 5 \times 5$ nm with periodic boundary conditions and filled it with 4107 TIP4P2005 water molecules at 300 K. Subsequently we used Nosé–Hoover thermostating to drive the temperature to one of the 19 target temperatures given in Table 5.1 and hold it there in all following simulations. The cubes with $T \geq 248.15$ K were equilibrated in this NVT-ensemble at the target temperature for 5 ns. Cubes with $T < 248.15$ K were equilibrated for 10 ns. Subsequently, like in [13], the z dimension of the simulation box was elongated to 20 nm. This slab system was then equilibrated for at least 10 ns, but significantly longer for lower temperatures. Following this second equilibration we started producing configurations for at least 50 ns. Since we used a Nosé–Hoover thermostat these configurations are distributed according to the canonical/NVT ensemble. The steps were integrated using the leapfrog algorithm with a time step of 1 fs. Total configurations containing positions, velocities and forces were saved every 1 ps. Energies – which were used in determining the surface tension – were saved every 0.1 ps. This process was repeated 5 times for each temperature in Table 5.1. All in all, the length of our MD-simulations combined exceeds 9.5 µs. A snapshot of the system at 298.15 K is shown in Fig. 3.2.

5.2 Methods of surface tension analysis

Turning now to the analysis of the resultant configurations; The macroscopic pressure tensor that GROMACS calculates with Eq. 3.14 for each saved energy of each temperature allows for the application of Eq. 2.4 to calculate the surface tension $\gamma(T)$. After we

Table 5.1: Details on the temperatures T and durations of equilibration and production of our MD-simulations. Equilibration times are given in the format: (*Time for cube equilibration* + *Time for slab system equilibration*)

T[K]	Equili.[ns]	Prod.[ns]
198.15	10 + 80	250
208.15	10 + 40	150
213.15	10 + 50	50
218.15	10 + 10	100
223.15	10 + 10	100
228.15	10 + 10	100
233.15	10 + 10	100
238.15	10 + 10	100
248.15	5 + 5	50
258.15	5 + 5	50
268.15	5 + 5	50
278.15	5 + 5	50
288.15	5 + 5	50
298.15	5 + 5	50
308.15	5 + 5	50
318.15	5 + 5	50
328.15	5 + 5	50
338.15	5 + 5	50
348.15	5 + 5	50

determined the statistical average of surface tension over the whole simulation time we applied three methods to analyse the result for the existence of an SIP.

5.2.1 Adjusting the IAPWS-equation

First, like Wang et al. [13] we fitted the IAPWS-equation (Eq. 2.5) to the results of surface tension for $T > 0\,°C$. We kept the critical exponent μ at $\frac{11}{9}$ [13] and used the method of least squares to determine the other parameters for the adjustment; $B = 206.2\,\mathrm{mN\,m^{-1}}$, $b = -0.557$ and a critical temperature $T_c = 661.543\,\mathrm{K}$. Comparing the extrapolation of the adjusted equation below 0 °C to our measurements makes it possible to determine if there is an anomalous rise or not.

5.2.2 Fermi function fit

Subsequent methods were applied to explore for an inflection of the surface tension.

First we fit a Fermi function over all measurements. The fit of this function was previously used by Sega et al. [52] to ascertain the temperature of the high-temperature inflection of surface tension (i.e. the first inflection point) in various water models,

including TIP4P2005. The Fermi function being:

$$F(x) = \frac{B}{1 - e^{C(x - x_{\text{inf}})}} + D, \tag{5.1}$$

where B, C, x_{inf} and D are fitting parameters. The inflection in F occurs at x_{inf} and D is a constant shift.

Equation 5.1 leaves open two possible scenarios by either identifying x with T or by identifying x with γ. We tried both possibilities and while both necessarily describe a monotonous function with an inflection, the predictions of these two fits lead to diametrically opposite scenarios. If our measurements were to follow $F(T)$, the relative increase of γ with a decrease of T would diminish at lower temperatures. By fitting $F(\gamma)$ the resultant curve fits the measurements much better, consistent with the SIP-proposal of an anomalous increase of surface tension.

5.2.3 Surface excess entropy

Following Wang et al. [13] we also calculated the surface excess entropy per unit area of our dataset. A sufficient condition for an inflection point at T_{inf} is a change of sign in $\frac{\mathrm{d}^2\gamma}{\mathrm{d}T^2}(T)$ on crossing T_{inf}. This in turn is equivalent to $\frac{\mathrm{d}\gamma}{\mathrm{d}T}(T)$ having a local extremum at T_{inf}. With Eq. 2.3 we can identify $-\frac{\mathrm{d}\gamma}{\mathrm{d}T}$ with the surface excess entropy $\frac{S_S}{\Sigma}$. A local extremum in $\frac{\mathrm{d}\gamma}{\mathrm{d}T}$ will thus be mirrored by a local extremum in $\frac{S_S}{\Sigma}$ at the identical temperature. Due to $\frac{S_S}{\Sigma}$ allowing for the search for an inflection while also possessing physical interest going beyond this feature, it will be the quantity of interest in the search for an SIP.

We used the method of central differences to calculate $\frac{\mathrm{d}\gamma}{\mathrm{d}T}$ for our datasets and for the Fermi function fit and plotted $\frac{S_S}{\Sigma}$ to search for local extrema.

5.3 Methods of structural analysis

A primary objective of our study was the distribution of high-density liquid (HDL) and low-density liquid (LDL) inside the slab and how it relates to other observables like the average number of neighbours and the number density, especially in the supercooled regime. For this purpose, we need to discuss criterions to label a particular molecule as HDL or LDL and how to build a profile of observables. We will also discuss the ITIM algorithm that allows us to discriminate molecules into different interfacial layers.

We made extensive use of the *Pytim*-package [88] in Python 3.7 to calculate profiles and for its implementation of the ITIM algorithm. Pytim itself expands upon the *MDAnalysis*-package [89, 90], which provides data structures to analyse files generated by MD-suites like the GROMACS 2019.3 [87] molecular dynamics package.

5.3.1 Profiling

To determine the distributions of observables in the slab as functions of distance from the center of mass in the normal direction, the system was cut into 0.2 nm wide bins. For

each such bin we calculated observables like density or HDL-fraction inside and separately statistically averaged the observables over all produced configurations in the production runs of Table 5.1.

5.3.2 ITIM algorithm

In addition to creating a profile of the whole system we also wanted to analyse separately the observables inside the first few layers. Among other reasons this would allow us to determine what layer(s) might be responsible for the high density anomaly, called the apophysis, right at the interface reported in past studies [15, 16, 17, 18, 19, 13].

An algorithm that can determine individual layers is ITIM (Identification of Truly Interfacial Molecules) [91]. In this algorithm, probe spheres are initialized outside the slab and moved in the normal direction toward the interface. The first molecules of the slab being hit by such a probe sphere are labelled as belonging to the first layer. The second layer can be determined by eliminating those molecules belonging to the first layer from the system and applying the algorithm once more [91], and so on for deeper layers. The process is depicted in Fig. 5.1. The ITIM-algorithm can only be applied to a planar interface. For another geometry a generalized version can be found in [92].

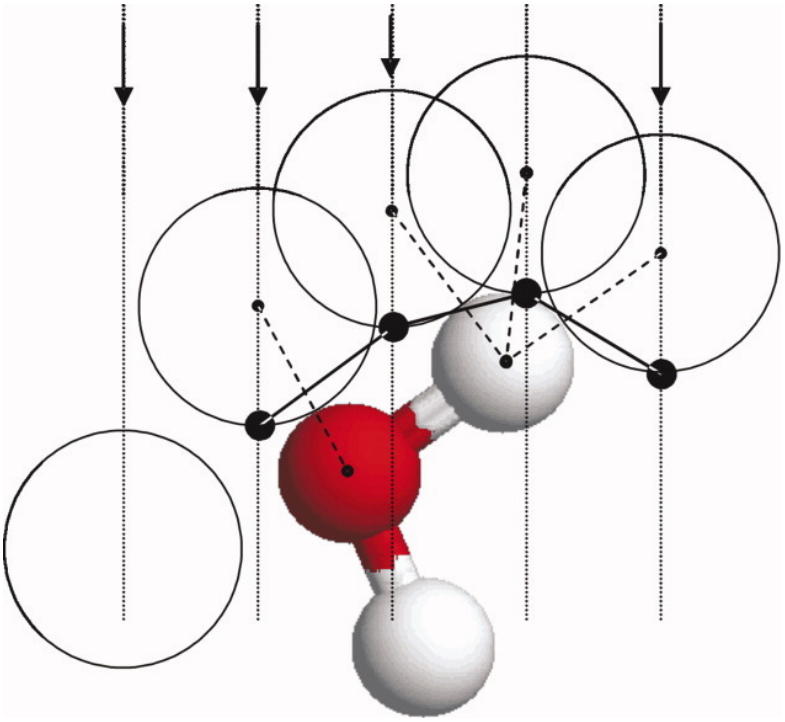

Figure 5.1: The ITIM-algorithm. The first molecule that collides with the probe spheres is set to belong to the first layer. The filled dots at the bottom of the probe spheres are used to estimate the position of the interfacial plane. Image reprinted from Pártay et al. [91].

5.3.3 HDL and LDL criterions

The eponymous difference of LDL and HDL is their low and respectively high density. While a markedly density-inhomogeneity in the profile of a water system may suggest the existence of a phase transition, the macroscopic density is too coarse of an indicator for almost all enquiries into LDL/HDL. In Chapter 6 we will even see that there are places and temperatures of the slab where the density and LDL-fraction of the system can simultaneously increase.

Our goal is an analysis of the structural properties of TIP4P2005 with respect to the HDL/LDL two-structure theories which necessitates us to measure the fractions of LDL and respectively HDL as profiles over a wide range of temperatures. For this the introduction of a microscopic criterion that can instantaneously classify a molecule as HDL or LDL is necessary.

Similar to the characteristic structures of LDA and HDA (Section 1.3), the LDL phase is characterized by having established a hydrogen bonding network and having fewer neighbours in the first coordination shell compared to HDL where there are additional molecules intruding into the network. As such there are differences in the local structures of the phases that can be quantified. A convenient criterion is the distance to the fifth nearest neighbour d_5 [93]. Since hydrogen bonds are possible with up to 4 interaction partners, one can categorize molecules with 4 or less neighbours into LDL and molecules with 5 or more into HDL.

Since liquids, unlike crystals, are not ordered in a lattice structure we need to clarify what we mean by neighbours. An essential property of neighbours should be the notion that they strongly interact with each other. A method that builds upon this notion was put forward by Stillinger to classify liquid clusters [94]. We start with identifying the interaction range r_S of the short ranged potential. At a distance below r_S the particles should interact significantly. In potentials with a sharp cutoff this may be identified with the cutoff itself. With r_S we can identify those particles as neighbours that are less than r_S apart.

For water we use the oxygen-oxygen distance between water molecules. The intermolecular interactions (Equations 4.1 and 4.2) also do not have a sharp cutoff. In these cases, a discussion of what constitutes a reasonable interaction range is necessary before applying the Stillinger-method. One choice is to estimate r_S from the minimum of the oxygen-oxygen pair correlation function that separates the first with the second coordination shell. This is the approach taken in the d_5-criterion in which Cuthbertson and Poole [93] have estimated a good cutoff to be $r_S = 3.5\,\text{Å}$.

The Stillinger-method is not the only approach to count neighbours and classify liquid clusters. A technique applicable to a wide variety of questions pertaining to liquid structure is the purely geometric method of Voronoi tessellation [95]. A method that aims to remove contribution of vapour-like neighbours, expanding upon the Stillinger method was proposed by ten Wolde and Frenkel [96, 97], where only those particles are counted that already have 5 neighbours. Finally, in determining water's structure there are several other order parameters that aim to quantify the tetrahedral order of a water molecule itself, without necessarily counting nearest neighbours [98].

6 Results and Discussion

Using the production runs of Chapter 5.1 we calculated the surface tension and structural profiles over all temperatures. We will present separately our results on the surface tension and the structural profiles before correlating them with each other and presenting a possible connection between the second inflection point (SIP) and the liquid-liquid transition (LLT).

6.1 Surface tension

Using Eq. 2.4 with $n = 2$ we calculated the surface tension using the pressure tensors from the production runs of Table 5.1. We plotted the result in Fig. 6.1 together with the results of a previous study of SPC/E and TIP4P2005 by Wang, Binder, Chen et al. [13] and recent experimental data by Vinš et al. [5]. Since we oriented our simulations toward Wang et al. – insofar as including the same temperatures – a very direct comparison is possible. The observations of Wang et al. and ours agree to a very high degree.

Like Wang et al. we fitted the IAPWS-equation (Eq. 2.5) with datapoints above 0 °C to adjust it to TIP4P2005. The extrapolation of this fit to sub-zero temperatures reveals an anomalous growth of surface tension that begins in the range of 238.15-248.15 K. Above 248.15 K the observations follow the extrapolated/adjusted IAPWS-fit very well, but below we – in analogy to Wang et al. [13] – see an ever growing divergence.

The SIP-proposal hypothesizes this anomalous rise at low T but also an actual inflection point of the surface tension. While the anomalous rise is readily apparent in Fig. 6.1, the hypothesized inflection is not visible at all. For this purpose, we applied two different analytical methods to comment on the possibility and location of an inflection.

In Fig. 6.2a we applied Fermi function fits of Eq. 5.1 to the complete temperature range of our data, Wang et al.'s simulation on SPC/E as well as Vinš et al.'s experimental data. We tried both $F(T)$ and $F(\gamma)$. $F(\gamma)$ fit the data much better, exactly follows the adjusted IAPWS-equation and also agrees with the extrapolation until 258.15 K. The inflection points of these Fermi function fits are respectively 282.62 K for our data, 268.90 K for Vinš et al. experiment and 249.28 K for Wang et al.'s simulation on SPC/E. The latter would agree with the findings of Wang et al. on the location of the SIP of SPC/E using the method of minimum of surface excess entropy per unit area, as they used it to suggest an inflection point between 240-250 K.

Figure 6.2b shows the surface excess entropy per unit area of our data, Wang et al.'s simulation on TIP4P2005 as well as Vinš et al.'s experimental data. The most striking result to emerge from this analysis is that the surface excess entropy per unit area attained by the temperature derivative leads to a minimum at 278.15 K, which

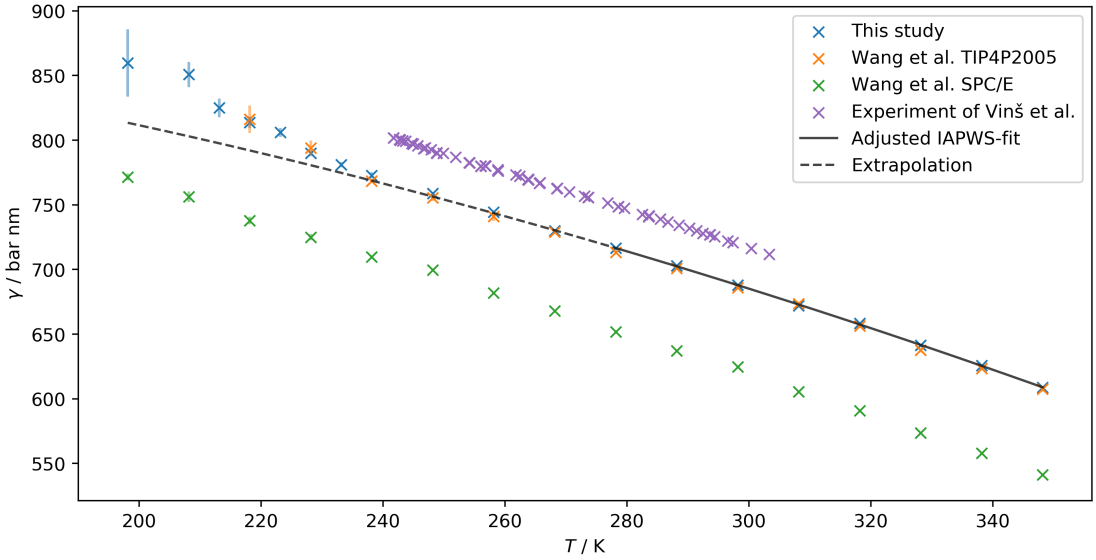

Figure 6.1: Surface tension as a function of temperature. Apart from this study the plot includes a study of Wang et al. [13] on two different models as well as recent experimental data by Vinš et al. [5]. The adjusted IAPWS-equation and its extrapolation is plotted in relation to our study.

together with the inflection of the Fermi function fit at 282.62 K would imply an inflection above 0 °C. The uncertainties in the temperature derivative however are large and get unfeasibly massive with falling T, such that the location of the minimum/inflection cannot be truly resolved. This is readily evidenced by Wang et al.'s data of the surface excess entropy of TIP4P2005. While our results and the calculations of Wang et al. agree within uncertainty, the minimum in the data of Wang et al. would fall 20 K lower. Applying a Fermi function fit on their data however results in an inflection point at 286.19 K, less than 4 K above the inflection in the Fermi function of this study.

An inflection at 278 K would coincide with the density maximum, whereas the lower inflection of Wang et al. could coincide with the Widom-line (Fig. 1.4). Regardless of location, since the IAPWS-equation in Fig. 6.1 is of concave form, the anomalous diverging growth highly suggests an inflection to happen.

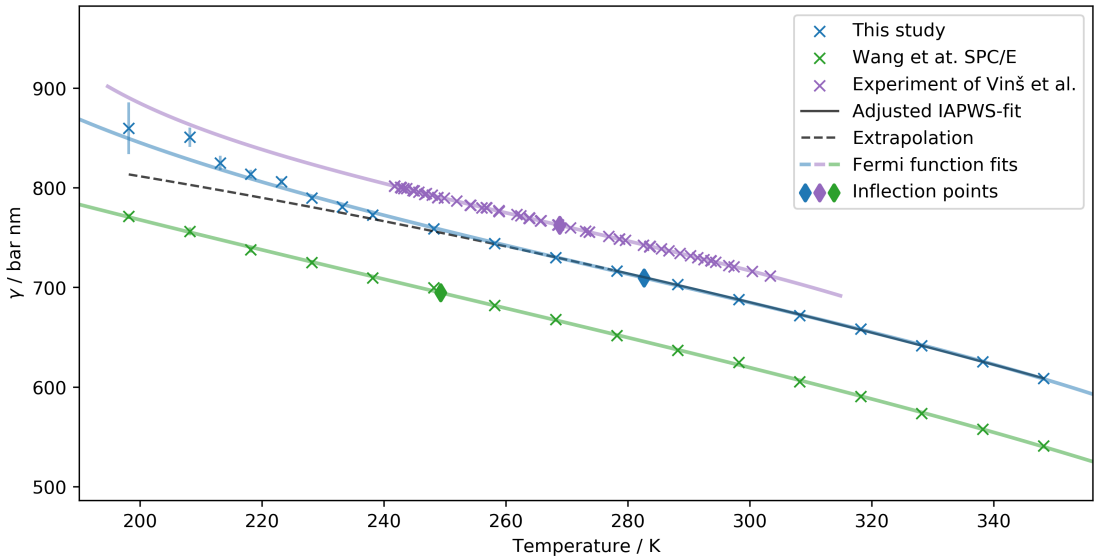

(a) Fermi functions of Section 5.2 fitted to our data, Wang et al.'s simulation on SPC/E and Vinš et al.'s experiment.

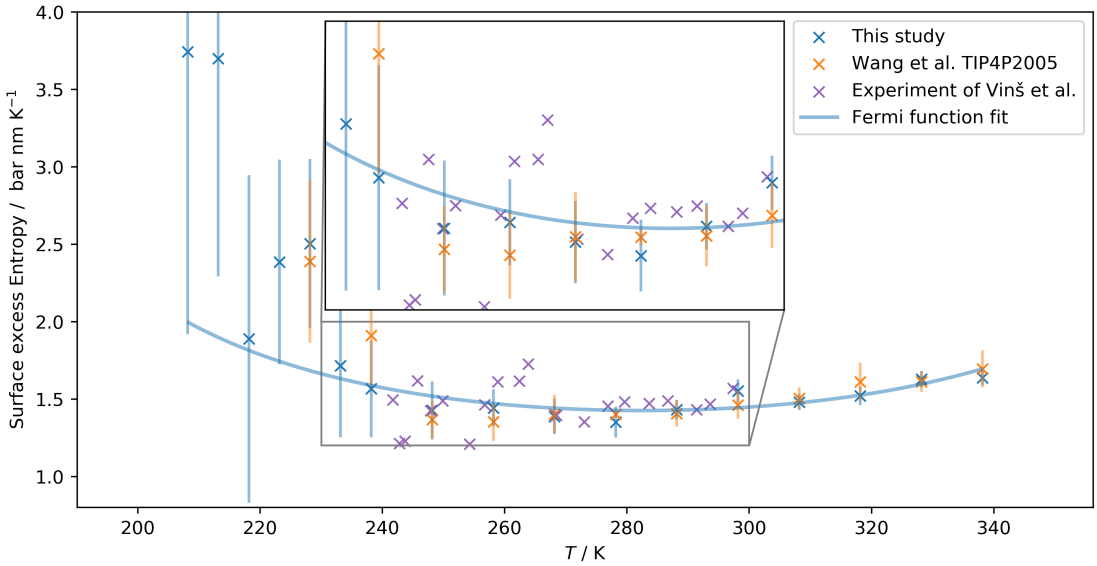

(b) Surface excess entropy of datapoints of surface tension as well as from this study's Fermi function fit. Uncertainties are symmetric.

Figure 6.2: Methods used to explore for an inflection point. For this study the inflection of the Fermi function fit falls at 282.62 K and the minimum of surface excess entropy at 278.15 K. For Wang et al.'s simulation on SPC/E the inflection of the Fermi function falls at 249.28 K and their minimum of $\frac{S_S}{\Sigma}$ between 240-250 K. Their simulation on TIP4P2005 would give a similar Fermi function like our study and an inflection point at 286.19 K, but the minimum of surface excess entropy is at 258.15 K.

6.2 Structural analysis

Using the trajectories obtained in Section 5.1 and the methods described in Section 5.3 we analysed the number density, the average number of neighbours as well as the HDL-fraction of the system. The profiles in this section are combined plots that emphasize broad changes in structure as we go from 348.15 K down to 198.15 K.

6.2.1 Density

By making use of the ITIM-algorithm (Section 5.3.2) implemented in Pytim [88] we detected the respective molecules of the first 4 layers. Using this distinction we plotted the density profile of the complete slab as well as the individual density profiles of the first four layers in Fig. 6.3. First and foremost, due to capillary waves the position of the layers is not constant, and we observe that the time average of the density profiles of different layers overlap. This explains why the maximal density of each layer – illustrated by the filled circles in Fig. 6.3 – falls so far below the density profile of the whole slab. By summing up the profiles of the individual layers, the total profile up until about the center of mass of layer III would be exactly retraced (not pictured).

In the density profiles at and below 248.15 K we see the formation of an anomalously high region of density below the surface. This is the apophysis that was reported by Matsubara et al. [15], Abe et al. [16], Haji-Akbari et al. [17], Haji-Akbari and Debenedetti [18], Malek et al. [19] and Wang et al. [13]. The latter study showed that the apophysis is not an artefact of insufficient simulation time and/or size.

Starting at 348.15 K, as we reduce the temperature, the density of all layers and of the full slab increases. This increase goes in hand with a contraction of the whole slab, which is visible in the movement of the layer's maxima (whose location in the normal direction is equivalent to the respective layers average center of mass). This behaviour stops around 278.15 K and reverses at 248.15 K as the slab begins to expand outwards. This temperature also coincides with a stagnation in the rise of the maximal density of layer III and IV whereas the already denser layer I continues to rise. Layer II (qualitatively) falls between layer I and III.

The contraction and expansion of the slab can be attributed to the density anomaly of water. In Fig. 6.4a we depicted the maximal densities of the layers together with the bulk mean density of the slab, where the *bulk* was defined as the region in the slab from -15 to 15 Å. The bulk mean density reaches a maximum of $0.0334\,\text{Å}^{-3}$ at 278.15 K, agreeing with the density maximum of TIP4P2005 at (278 ± 3) K for a pressure of 1 bar [79] and almost coinciding with the density anomaly of real water at 277.15 K.

Included in Fig. 6.4a is also the maximal density of the distributional sum of layers I and II. This is equivalent to the height of the apophysis. We notice that the growth of the height of the apophysis is almost mirrored in the growth observed in the maximal density of layer I, both increasing linearly, undisturbed by the contraction and expansion of the slab.

To establish a different perspective on layer densities we also calculated the integral of the density profiles of layers I - IV in Fig. 6.4b. This is a direct measure of the number

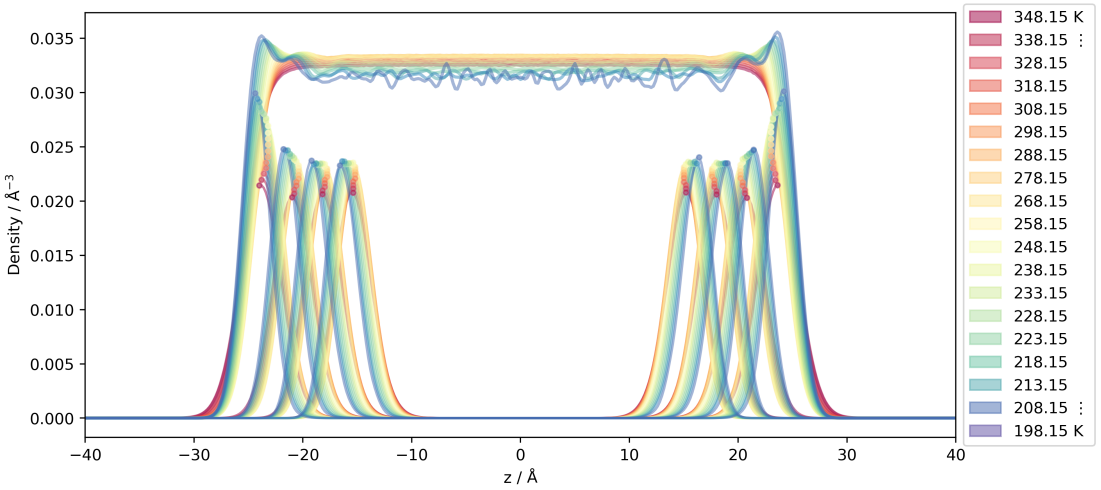

Figure 6.3: Density Profiles of the slab and the first four layers for the Production runs of Table 5.1. Centered is the liquid phase at 0 Å and the two interfaces are visible further outward. The outermost bell-like curves represent layer I of each interface, the one after layer II and so on. The circles denote the respective density maximum of the first four layers. The position of maximum density coincides with the center of mass of the density distributions.

of particles in each layer in units of a surface density. Canonically, layer I has the highest such density. But in opposition to their density maxima, these surface densities decrease monotonically with temperature in each layer. This needs to be attributed to the density distributions of each layer narrowing (implying flatter layers) with falling temperature. Interestingly, the surface density of the bulky layer IV does not decrease as much as the layers above. At 258.15 K it attains a higher surface density than layer III and also achieves a similar maximal density.

The formation of the apophysis can be connected to a compactification of layer I. With the surface density of layer I staying almost constant in comparison to the layers below, the continuing sharpening in its profile, combined with the decrease of bulk density leads to the apophysis at and below 248.15 K.

6.2.2 Distribution of neighbours

The number of neighbours of each molecule were calculated by counting the number of oxygen atoms that are less than the distance $r_S = 3.5$ Å away from each oxygen atom (see Section 5.3.3). The distribution of the average number of neighbours for different temperatures is pictured in the profiles of Fig. 6.5a.

By combining the knowledge of how many neighbours any molecule has and the labelling of what layer it is part of using ITIM, we were also able to make additional profiles for the average number of neighbours for molecules of each layer separately, as

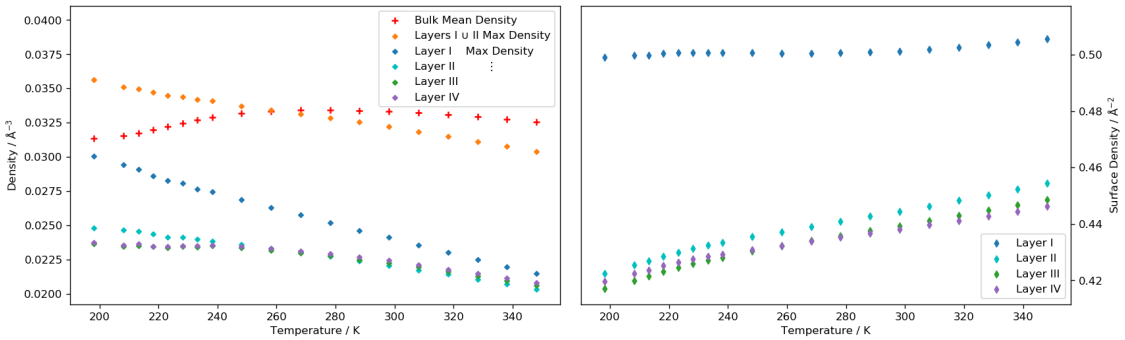

(a) Bulk density and density maxima of layers.

(b) Integrated density profiles of layers.

Figure 6.4: Bulk mean density, different density maxima and surface densities as functions of temperature.

shown in Fig. 6.5b.

Finally, by restricting the counting of neighbours to only those molecules that share the same layer we made the profiles of Fig. 6.5c. To put it in other words, Fig. 6.5c shows the contribution of neighbours of the same layer to the total layer-wise profiles of Fig. 6.5b. In turn, the weighted sum of Fig. 6.5b would exactly retrace the total profile of Fig. 6.5a until about the position of layer III.

Figure 6.5c could more accurately represent the two-dimensional structuring inside the layers since a possible interference of layers above and below the layer is removed. In particular, while the molecules of layer I evidently have the least number of neighbours (see Fig. 6.5b) of any layer, they consistently have more intralayer neighbours than any other. This and the fact that the first layer is the most compact (in regards to density maximum and total population) suggests that the comparatively small number of neighbours of the first layer pictured in Fig. 6.5b is to the highest degree the result that by simply being the first layer, its molecules can only have neighbours within itself or with the second layer.

The overall trend of the average number of neighbours in the total slab of Fig. 6.5a as well as in the layers II to IV is to decrease with temperature. In the first layer however, the number of neighbours stays roughly constant when compared to the layers below or to the slab. Finally, in total defiance of the layers below, its intralayer neighbours *rise* with sinking temperature. This conforms with our suggestion born from Fig 6.4a that the apophysis of Fig. 6.3 can be predominantly attributed to layer I.

An observation which may however suggest this to be a different phenomenon is that until at least 248.15 K the maximal density of the layers II to IV also seems to rise, but this is not mirrored in a rise in their intralayer neighbour profile. While this hinders us to make a direct connection between density and intralayer neighbours, it at least illustrates that while a local density as given in the number of neighbours (Fig. 6.5) and the total density (Fig. 6.3) are related concepts, they do not have to be proportional and can even be anti-proportional.

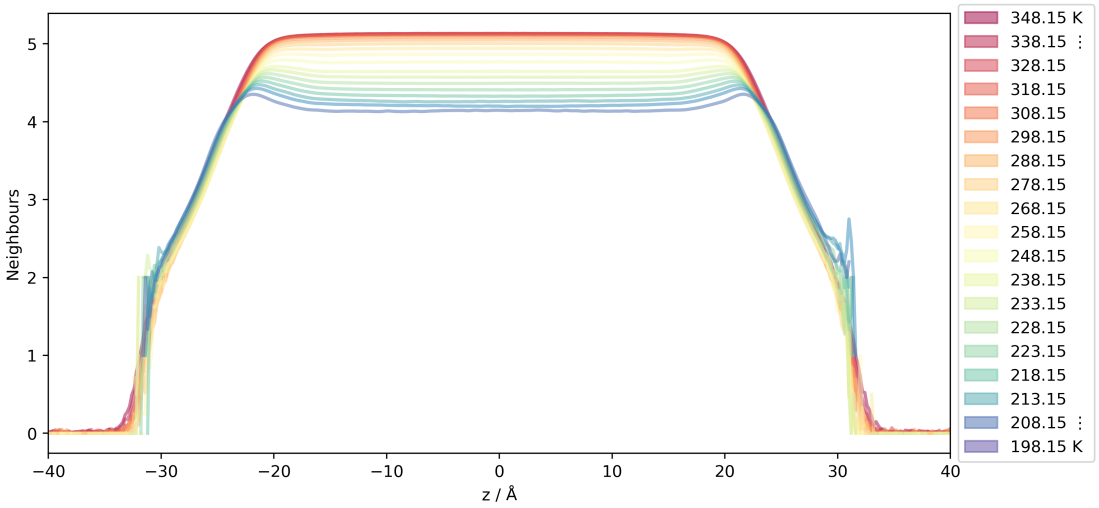

(a) Average neighbour profiles of the system.

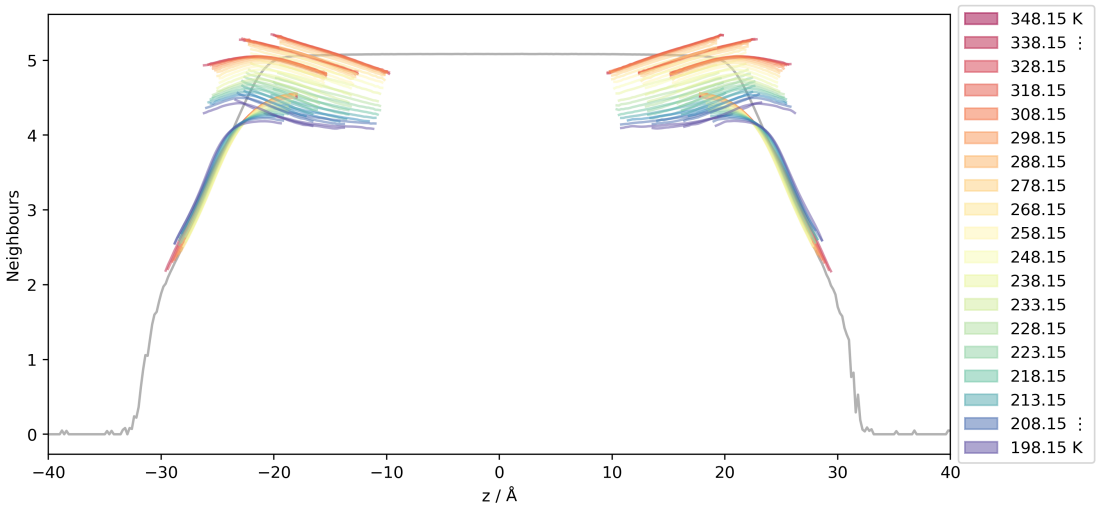

(b) Average neighbour profiles of layers I - IV. The grey underlay is the profile at 298.15 K.

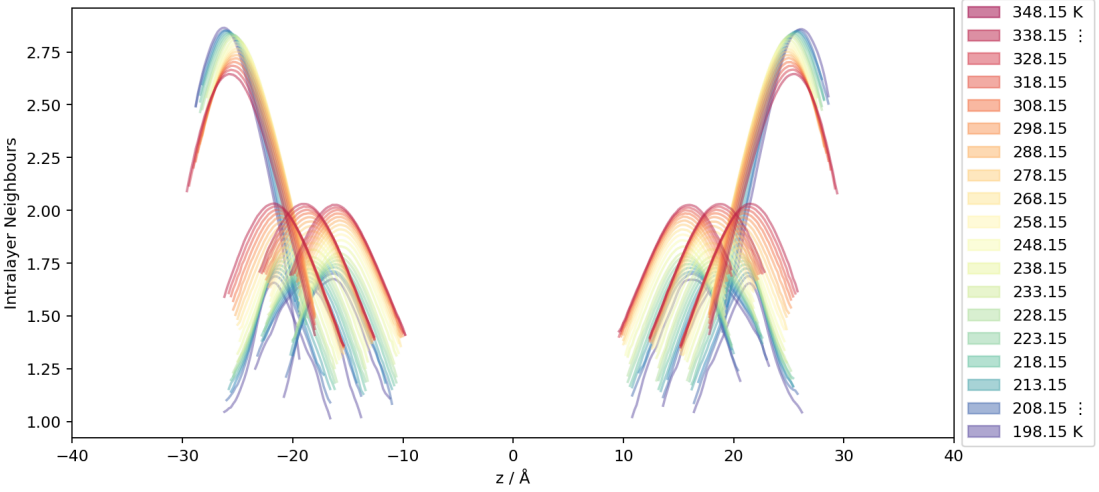

(c) Average intralayer neighbour profiles of layers I - IV.

Figure 6.5: Profiles of the average number of neighbours.

6.2.3 High density fraction

The determination of neighbours in Section 6.2.2 immediately allows for the application of the d_5-criterion to classify them as HDL if they have 5 or more neighbours and LDL otherwise. This allowed us to create profiles of the HDL-fraction in the system pictured in Fig. 6.6.

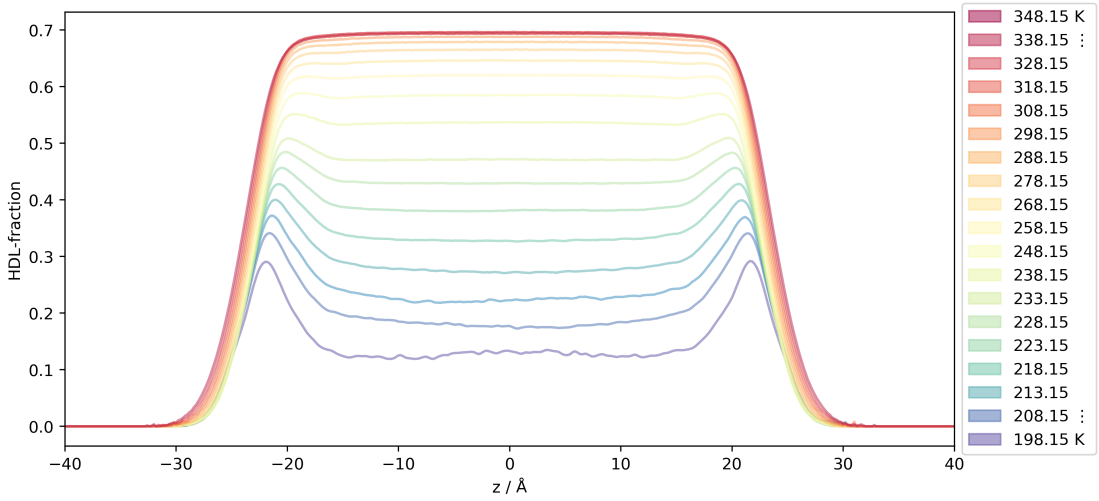

Figure 6.6: Profiles of the HDL-fractions. A maximal HDL-fraction forms in layer II but also layer III exhibits an HDL-fraction above the bulk below 233.15 K.

The overall trend is that with sinking temperature, HDL gets converted into LDL. The conversion starts slow at high T but speeds up the lower the temperatures become. Intriguingly, this conversion does not happen evenly across the slab. At 248.15 K we notice the formation of a region of anomalously high HDL-fraction directly under the surface. To be more precise, the conversion of HDL into LDL is slower in layer II, insofar as that at and below 248.15 K the mean HDL-fraction of layer II surpasses the bulk value. At particularly low temperatures even in layer III a HDL-fraction above bulk values is observed. The higher relative HDL-fraction at the interface implies a higher average number of neighbours which is visible in Fig. 6.5a.

In Fig. 6.7 we see more clearly the different speeds of conversion of HDL into LDL in the bulk and in layer II (the bulk being defined by the average HDL-fraction between -15 and 15 Å). At high temperatures the bulk HDL-fraction is greater than in layer II. Above 300 K the fractions even seem to stay constant with T. Upon lowering the temperature, the bulk fraction drops faster than layer II, insofar as being surpassed by it between 248-258 K. Layer III shows a similar albeit weaker divergence. Layer IV already shows minimal divergence to bulk behaviour.

Due to neither layer II exhibiting anomalous behaviour in its profile of intralayer neighbours, nor layer II or layer III showing a markedly different trend in their density, as compared to the already very bulky layer IV, we suspect that the reason for this

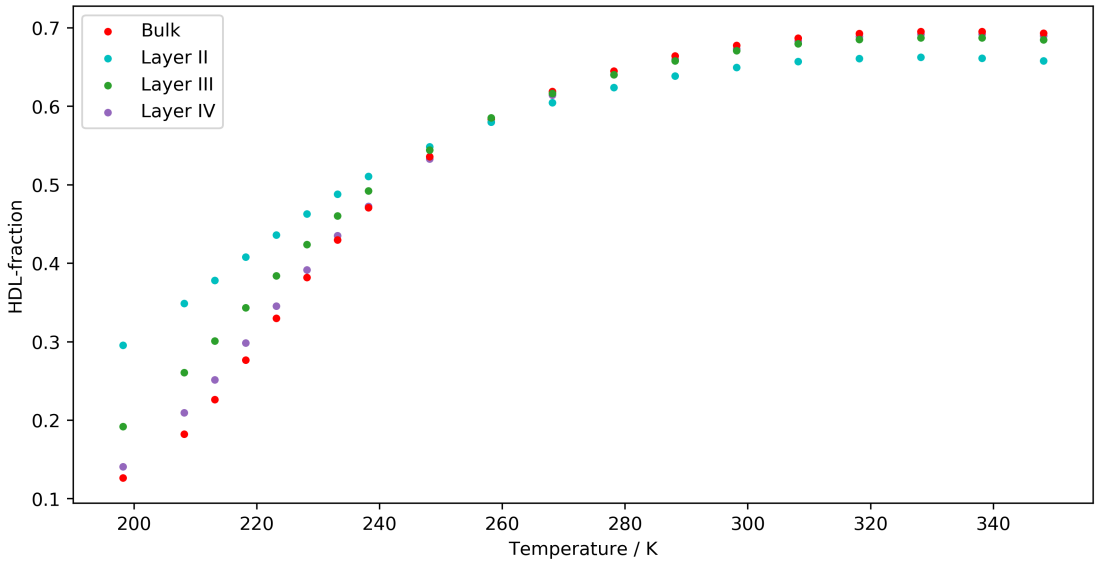

Figure 6.7: HDL-fractions as functions of temperature. The conversion of HDL into LDL in layer II is slower than in the bulk. Layer III and arguably even IV show a similar albeit weaker behaviour.

seemingly enrichment of HDL in layer II is to a high degree actually due to the compactification of layer I.

Since layer I is the interfacial layer, the direct application of the d_5-criterion to infer its HDL-fraction does not give a meaningful answer, if a meaningful answer of HDL/LDL on the interfacial layer is even possible. A rescaling of the criterion at surfaces should be debated. But even without knowing definitely whether the first layer would follow an HDL or LDL enrichment, the enrichment of the still quite interfacial layer II is observed.

Malek et al. have also observed the appearance of the apophysis [99] together with a relative increase of neighbours at the surface in comparison to the bulk [19] in their research of TIP4P2005 water droplets. Using a local tetrahedral order parameter, they also quantified this enrichment with a breakdown of tetrahedral structure.

The density anomaly which results in the center of mass of the first layers moving inwards until about 278.15 K before racing outwards after around 248.15 K could be attributed to the conversion of HDL into LDL. At high temperature there is only a relatively small conversion of HDL into LDL. As the slabs temperature is lowered the behaviour is that of an ordinary liquid and it contracts, leading to an increase of the density in the bulk. This process continues but slows down until stopping at around 278.15 K. At 248.15 K the conversion of HDL into LDL is fast and since LDL as the icelike component of the mixture uses more volume than HDL the contraction due to cooling is trumped by an outward expansion due to a higher fraction of LDL, leading to a considerable decrease in density.

6.3 Correlation between surface tension and HDL-fraction

To connect our findings of structure with the anomalous growth of surface tension we calculated the Pearson correlation between the fluctuations in surface tension and the fluctuations in HDL-fraction by calculating block averages of 50 ps of these quantities in the production runs of Table 5.1. The size and significance of the coefficients for the HDL-fractions of the total slab and of layer II may justify using linear fits of the fluctuating values to estimate the derivatives of surface tension with the respective HDL-fraction. The results are listed in Table 6.1.

Table 6.1: The Pearson coefficients between the fluctuations of HDL-fraction x_{HDL} and the fluctuations of surface tension γ calculated for the HDL-fractions of the total slab and for layer II. The derivatives $\frac{\mathrm{d}\gamma(T)}{\mathrm{d}x_{\mathrm{HDL}}(T)}$ were estimated from the slopes of the linear fits between surface tension and respective HDL-fraction.

	Total slab		Layer II	
T [K]	Pearson coeff.	$\frac{\mathrm{d}\gamma(T)}{\mathrm{d}x_{\mathrm{HDL}}(T)}$ [bar nm]	Pearson coeff.	$\frac{\mathrm{d}\gamma(T)}{\mathrm{d}x_{\mathrm{HDL}}(T)}$ [bar nm]
198.15	−0.03	$(1 \pm 6) \cdot 10^2$	−0.10	$(-15 \pm 3) \cdot 10^2$
208.15	−0.11	$(-23 \pm 4) \cdot 10^2$	−0.09	$(-10 \pm 3) \cdot 10^2$
213.15	−0.23	$(-40 \pm 6) \cdot 10^2$	−0.12	$(-13 \pm 4) \cdot 10^2$
218.15	−0.13	$(-21 \pm 4) \cdot 10^2$	−0.10	$(-12 \pm 3) \cdot 10^2$
223.15	−0.19	$(-26 \pm 3) \cdot 10^2$	−0.12	$(-13 \pm 3) \cdot 10^2$
228.15	−0.24	$(-30 \pm 3) \cdot 10^2$	−0.16	$(-16 \pm 3) \cdot 10^2$
233.15	−0.26	$(-30 \pm 3) \cdot 10^2$	−0.17	$(-16 \pm 3) \cdot 10^2$
238.15	−0.29	$(-32 \pm 4) \cdot 10^2$	−0.19	$(-17 \pm 3) \cdot 10^2$
248.15	−0.35	$(-40 \pm 4) \cdot 10^2$	−0.21	$(-18 \pm 3) \cdot 10^2$
258.15	−0.40	$(-51 \pm 4) \cdot 10^2$	−0.21	$(-19 \pm 3) \cdot 10^2$
268.15	−0.38	$(-56 \pm 5) \cdot 10^2$	−0.21	$(-19 \pm 3) \cdot 10^2$
278.15	−0.38	$(-63 \pm 5) \cdot 10^2$	−0.17	$(-16 \pm 4) \cdot 10^2$
288.15	−0.36	$(-63 \pm 6) \cdot 10^2$	−0.18	$(-18 \pm 4) \cdot 10^2$
298.15	−0.39	$(-78 \pm 6) \cdot 10^2$	−0.17	$(-18 \pm 4) \cdot 10^2$
308.15	−0.38	$(-81 \pm 7) \cdot 10^2$	−0.15	$(-16 \pm 4) \cdot 10^2$
318.15	−0.37	$(-82 \pm 7) \cdot 10^2$	−0.16	$(-17 \pm 4) \cdot 10^2$
328.15	−0.36	$(-83 \pm 7) \cdot 10^2$	−0.14	$(-15 \pm 4) \cdot 10^2$
338.15	−0.33	$(-79 \pm 8) \cdot 10^2$	−0.12	$(-12 \pm 4) \cdot 10^2$
348.15	−0.32	$(-78 \pm 8) \cdot 10^2$	−0.13	$(-13 \pm 4) \cdot 10^2$

We found the fluctuations of HDL-fraction of the whole slab as well as respectively of the second layer and of the bulk to have a significant negative correlation with surface tension. A higher HDL-fraction always coincided with a lower surface tension.

This indicates the possibility of the two structures to have separate, inequal molar contributions to the surface tension with $\gamma_{\mathrm{LDL}}(T) > \gamma_{\mathrm{HDL}}(T)$. This would imply that the SIP may come about due to the conversion of the predominantly HDL system at high

temperatures into the predominantly LDL as we approach and cross the Widom-line in the supercooled regime. After the system is already made up of LDL the exponential deviation to the IAPWS-extrapolation might cease. A similar argument has been made by Rogers et al. [14] for the WAIL model of water; in which an observed exponential deviation to the IAPWS-extrapolation might originate in an exponential increase of LDL as the temperature approaches the Widom-line.

Unequal molar surface tensions might also be related to the formation of the apophysis. In a binary mixture the surface is enriched in the component of lower surface tension, since this minimizes the free energy [100]. Supposing $\gamma_{\mathrm{LDL}} > \gamma_{\mathrm{HDL}}$ holds this would lead to the enrichment of HDL in the interfacial region observed in the previous section. The enrichment of HDL would in turn result in a region of higher density and bring about the apophysis. This explanation cannot however address why the apophysis starts to appear at 248.15 K, since the correlations in Table 6.1 would imply HDL to be favoured at every temperature.

To explore the hypothesis that inequal molar surface tensions of LDL and HDL unify the anomalies of the SIP and the apophysis with the LLT, we investigated the model of an ideal binary mixture in which the total surface tension is linearly partitioned into two molar surface tensions:

$$\gamma(T) = \gamma_{\mathrm{HDL}}(T) \cdot x_{\mathrm{HDL}}(T) + \gamma_{\mathrm{LDL}}(T) \cdot \big(1 - x_{\mathrm{HDL}}(T)\big), \tag{6.1}$$

with x_{HDL} being the HDL-fraction of the interfacial layer. Since the d_5-criterion breaks down at layer I we approximated x_{HDL} with the HDL-fraction of the total slab and with the HDL-fraction of layer II. With only Eq. 6.1, the molar surface tensions are indeterminate. The significant Pearson coefficients of Table 6.1 may however justify linearly fitting the fluctuations between $\gamma(T)$ and the respective $x_{\mathrm{HDL}}(T)$ for each T. The slopes of these fits are given in Table 6.1, serving as estimators of the derivative of surface tension with respect to HDL-fraction. With these values and the derivative of Eq. 6.1

$$\frac{\mathrm{d}\gamma(T)}{\mathrm{d}x_{\mathrm{HDL}}(T)} = \gamma_{\mathrm{HDL}}(T) - \gamma_{\mathrm{LDL}}(T), \tag{6.2}$$

the molar surface tensions of the model become determinate. We plotted the results following from the HDL-fraction of layer II in Fig. 6.8a and from the total HDL-fraction in Fig. 6.8b.

In Fig. 6.8a the molar surface tension γ_{HDL} seems to stay rather constant whereas γ_{LDL} first rises to a maximum between 268.15 K to 298.15 K before falling again. Due to $\frac{\mathrm{d}\gamma(T)}{\mathrm{d}x_{\mathrm{HDL}}(T)} < 0$ for all T, the supposed property $\gamma_{\mathrm{LDL}} > \gamma_{\mathrm{HDL}}$ is fulfilled everywhere. A big shortfall of the result are the highly unusual trends of the molar surface tensions. The large derivatives in Table 6.1 lead to considerable differences in the values of γ_{LDL} and γ_{HDL}, the latter of which takes on very small values. Furthermore, the molar surface tensions seem to be somewhat inversely proportional to each other over a wide range of temperatures and we fail to offer an explanation for this behaviour. The decrease of γ_{LDL} in temperatures below 268.15 K is highly anomalous in its own right. This may serve as an indication of shortcomings in the model.

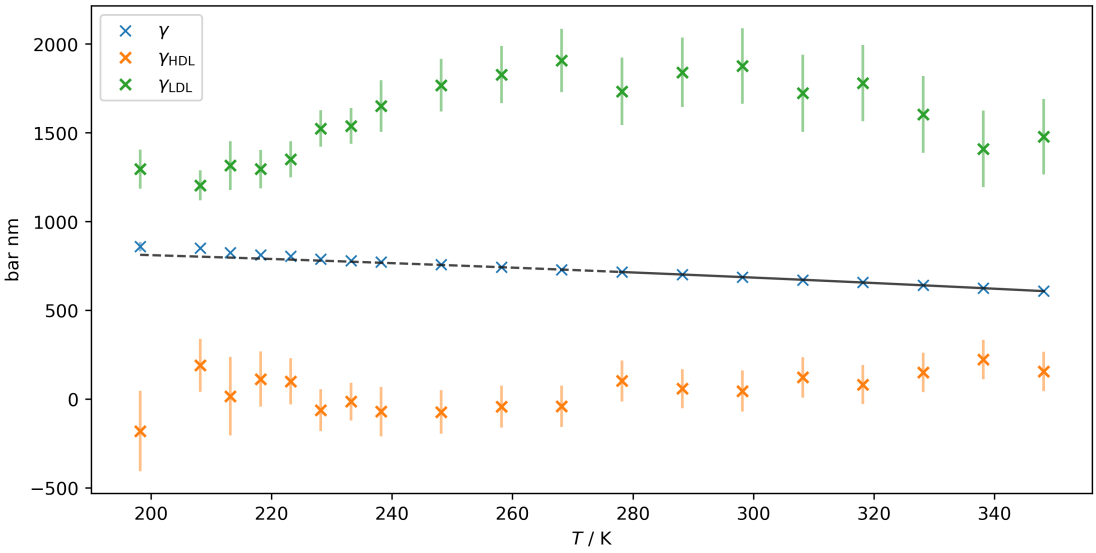

(a) Molar surface tensions γ_{HDL} and γ_{LDL} calculated using the HDL-fraction of layer II.

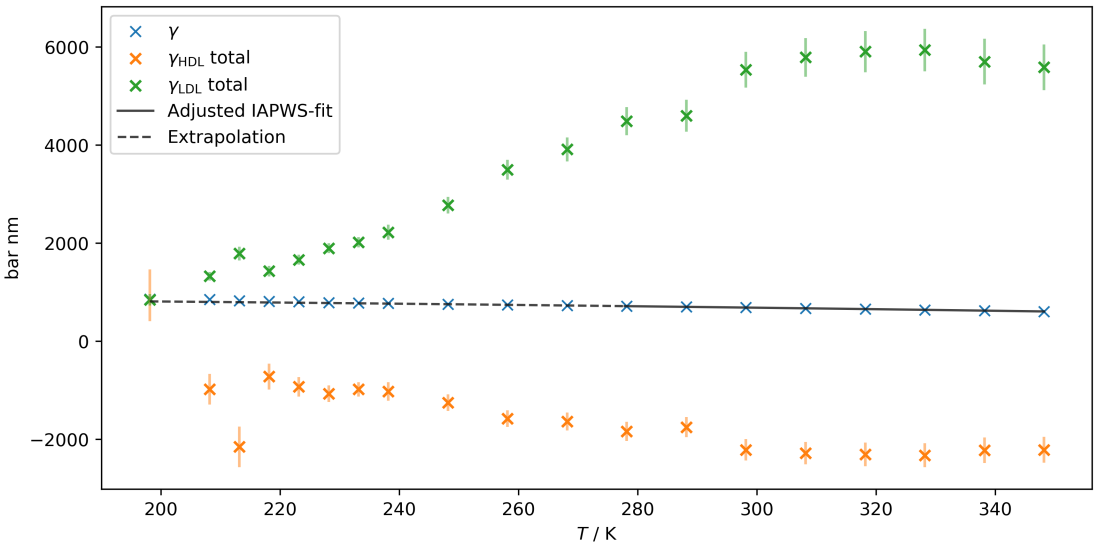

(b) Molar surface tensions γ_{HDL} and γ_{LDL} calculated using the HDL-fraction of the total slab.

Figure 6.8: Molar surface tensions γ_{HDL} and γ_{LDL} calculated through Eq. 6.1 and Eq. 6.2 using the derivatives in Table 6.1.

In the case of Fig. 6.8b, which follows from using the total HDL-fraction instead of the HDL-fraction of layer II, the molar surface tensions seem to stay constant until 298.15 K, below which they almost monotonically rise in the case of γ_{HDL} and fall in the case of γ_{LDL}. The supposed property $\gamma_{\text{LDL}} > \gamma_{\text{HDL}}$ is fulfilled everywhere except at 198.15 K. Again, big shortfalls of the result are the highly unusual trends of the molar surface tensions.

The derivatives are extremely large, leading to enormous differences in the values of γ_{LDL} and γ_{HDL}, the latter taking on negative values throughout. In similarity to Fig. 6.8a, the molar surface tensions seem to be somewhat inversely proportional to each other and a kindred decrease of γ_{LDL} in a wide range of lower temperatures is observed. This may serve as further indication of shortcomings in the approach.

Equation 6.1 may be too stark of an idealization of the actual behaviour, the Pearson coefficients may be too small to allow for proper linear fits, Eq. 6.1 may only be the very first term in a two-structure equation of surface tension or the hypothesis may be misguided altogether.

An undertaking to explore this further could be to record the full atomistic pressure tensor and to separately sum up the individual contributions of HDL and LDL to the total pressure which could result in a direct estimate for γ_{HDL} and γ_{LDL}. Also, while simulations of the surface tension of TIP4P2005 below 198.15 K are difficult, it would be interesting to see if the exponential deviation continues or, as the system is expected to stay predominantly LDL, if it ceases.

Theoretical approaches into the surface tension of TIP4P2005 using HDL/LDL two-structure theories and going beyond the linear terms of Eq. 6.1, could prove particularly valuable in gaining more insight into the SIP, the apophysis and their relation to the LLT.

A particular shortcoming of the study is that while we record the first layer as the most compact layer, we cannot effectively resolve its HDL-fraction because it being the interfacial layer will always result in a low HDL-fraction when using the d_5-criterion. In determining the molar surface tension through Eq. 6.1 and the derivative of surface tension with respect to HDL-fractions, we were left with the approximations that are the HDL-fractions of layer II, of the bulk or of the total system. The calculations using the bulk and the total system yield similar results, but these are not consistent with the results following the HDL-fraction of layer II. An improved calculation may therefore necessitate the HDL-fraction of the actual interfacial layer. The application of a different criterion to define the HDL-component (examples given at the end of Section 5.3.3) or rescaling the number of neighbours of the first layer to purposed bulk values would be an interesting study to see.

Conclusions and Outlook

The aim of the present research was to explore structural properties such as the HDL-fraction inside an interfacial vapour-water system and to specifically comment on the anomalies of the SIP and the apophysis in the supercooled regime and their possible connection.

Our data was gathered using MD-simulations on a slab system of TIP4P2005 in the range of 198.15 to 348.15 K. The calculated surface tension as a function of temperature shows an anomalous divergence over the IAPWS-extrapolation below 248.15 K that is highly suggestive of an SIP. Both the surface excess entropy per unit area as well as a Fermi function fit locate the inflection point at about 278 K. This temperature happens to coincide with the observed density maximum but is 20 K higher than the minimum of surface excess entropy per unit area in the past study of Wang et al. [13].

Making use of the Stillinger method to count neighbours, the d_5-criterion to distinguish HDL from LDL and the ITIM-algorithm to determine the first four layers, we have examined the structure of the system. In particular, we have observed the appearance of the apophysis below 258.15 K to coincide with layer I getting more compact; in the sense that the maximal density as well as the number of intralayer neighbours of this layer increases while its total population stays roughly constant.

We also noticed that while the overall HDL-fraction decreases with falling temperature, it does not do so in a uniform fashion. The decrease becomes less pronounced in layer II and to a lesser degree in layer III, leading to a region of anomalously high HDL-fraction under the surface in the deeply supercooled regime. Since a compactification of the first layer could naturally lead to an increase in the neighbours of the second layer, this enrichment of HDL might be the same effect as the apophysis.

While it was not possible to assess a direct connection between the LLT, the SIP and the apophysis, the negative correlation between the fluctuations of HDL-fraction and surface tension was an unexpected insight that opens up related questions in need for further exploration. As the anomalous rise in surface tension coincides with a steep fall in HDL-fraction, this correlation indicates the possibility that the SIP originates in the conversion of HDL into LDL, and thus has its origin in the approach to the Widom line of the LLT in similarity to a study on WAIL by Rogers et al. [14]. Further yet, the apophysis might also be a result of the disparity in the molar surface tensions of HDL and LDL. In an ideal binary mixture, the enrichment of the surface in the phase of lower surface tension minimizes the free energy of the system. Due to HDL being negatively correlated with surface tension, it might thus be energetically favourable to have it on the surface, which would explain the enrichment of HDL in layer II and in turn, due to the higher relative density of HDL, lead to the apophysis. A theoretical approach into the surface tension of TIP4P2005 using HDL/LDL two-structure theories and going beyond the linear

terms of Eq. 6.1, could prove valuable in getting a more unified view of the possible connection between the anomalies in the supercooled regime.

A shortcoming of the study is that while we record the first layer as the most compact layer, we cannot effectively resolve its HDL-fraction because it being the interfacial layer will always result in a low HDL-fraction when using the d_5-criterion. We have thus not been able to study the enrichment of HDL in the first layer, correlate its fluctuations with surface tension nor use its HDL-fraction in Eq. 6.1. Therein approximating the HDL-fraction of layer I with the HDL-fraction of layer II or the HDL-fraction of total system yielded inconsistent and unusual values for the molar surface tensions. An improved calculation may therefore necessitate the HDL-fraction of the actual interfacial layer. The application of a different criterion to define the HDL-component or rescaling the number of neighbours of the first layer to purposed bulk values would be an interesting study to see.

Another undertaking could be to record the full atomistic pressure tensor and to separately sum up the individual contributions of HDL and LDL to the total pressure which could result in a direct estimate for γ_{HDL} and γ_{LDL}. Additionally, while simulations of the surface tension of TIP4P2005 below 198.15 K become particularly difficult due to slow relaxation, it would be interesting to see if the exponential deviation of the surface tension continues or, as the system should stay predominantly LDL, if it ceases.

Bibliography

[1] D. Rosenfeld and W. L. Woodley. "Deep convective clouds with sustained supercooled liquid water down to - 37.5 °C". *Nature* 405.6785 (May 2000), pp. 440–442. DOI: 10.1038/35013030.

[2] R. Skogseth, F. Nilsen, and L. H. Smedsrud. "Supercooled water in an Arctic polynya: Observations and modeling". *Journal of Glaciology* 55.189 (2009), pp. 43–52. DOI: 10.3189/002214309788608840.

[3] Y. Song, R. Sharp, F. Lu, and M. Hassan. "The future potential of cryopreservation for assisted reproduction". *Cryobiology* 60.3 SUPPL. (July 2010), S60–S65. DOI: 10.1016/j.cryobiol.2009.09.009.

[4] J. C. Palmer, P. H. Poole, F. Sciortino, and P. G. Debenedetti. *Advances in Computational Studies of the Liquid-Liquid Transition in Water and Water-Like Models*. Sept. 2018. DOI: 10.1021/acs.chemrev.8b00228.

[5] V. Vinš, J. Hykl, J. Hrubý, A. Blahut, D. Celný, et al. "Possible Anomaly in the Surface Tension of Supercooled Water: New Experiments at Extreme Supercooling down to -31.4 °C". *The journal of physical chemistry letters* 11.11 (June 2020), pp. 4443–4447. DOI: 10.1021/acs.jpclett.0c01163.

[6] H. R. Pruppacher and J. Klett. *Microphysics of clouds and precipitation*. Springer, Dordrecht, 2010. DOI: https://doi.org/10.1007/978-0-306-48100-0.

[7] P. H. Poole, R. K. Bowles, I. Saika-Voivod, and F. Sciortino. "Free energy surface of ST2 water near the liquid-liquid phase transition". *Journal of Chemical Physics* 138.3 (Jan. 2013), p. 034505. DOI: 10.1063/1.4775738. arXiv: 1212.1600.

[8] J. C. Palmer, F. Martelli, Y. Liu, R. Car, A. Z. Panagiotopoulos, et al. "Metastable liquid-liquid transition in a molecular model of water". *Nature* 510.7505 (June 2014), pp. 385–388. DOI: 10.1038/nature13405.

[9] F. Smallenburg and F. Sciortino. "Tuning the Liquid-Liquid Transition by Modulating the Hydrogen-Bond Angular Flexibility in a Model for Water". *Physical Review Letters* 115.1 (July 2015), p. 015701. DOI: 10.1103/PhysRevLett.115.015701.

[10] R. S. Singh, J. W. Biddle, P. G. Debenedetti, and M. A. Anisimov. "Two-state thermodynamics and the possibility of a liquid-liquid phase transition in supercooled TIP4P/2005 water". *Journal of Chemical Physics* 144.14 (Apr. 2016). DOI: 10.1063/1.4944986. arXiv: 1602.04242.

[11] P. H. Handle and F. Sciortino. "Potential energy landscape of TIP4P/2005 water". *Journal of Chemical Physics* 148.13 (Apr. 2018), p. 134505. DOI: 10.1063/1.5023894. arXiv: 1802.02810.

[12] Y. J. Lü and B. Wei. "Second inflection point of water surface tension". *Applied Physics Letters* 89.16 (Oct. 2006), p. 164106. DOI: 10.1063/1.2364167.

[13] X. Wang, K. Binder, C. Chen, T. Koop, U. Pöschl, et al. "Second inflection point of water surface tension in the deeply supercooled regime revealed by entropy anomaly and surface structure using molecular dynamics simulations". *Physical Chemistry Chemical Physics* 21.6 (Feb. 2019), pp. 3360–3369. DOI: 10.1039/C8CP05997G.

[14] T. R. Rogers, K. Y. Leong, and F. Wang. "Possible Evidence for a New Form of Liquid Buried in the Surface Tension of Supercooled Water". *Scientific Reports* 6.1 (Sept. 2016), pp. 1–6. DOI: 10.1038/srep33284.

[15] H. Matsubara, T. Koishi, T. Ebisuzaki, and K. Yasuoka. "Extended study of molecular dynamics simulation of homogeneous vapor-liquid nucleation of water". *Journal of Chemical Physics* 127.21 (Dec. 2007), p. 214507. DOI: 10.1063/1.2803899.

[16] K. Abe, T. Sumi, and K. Koga. "Temperature dependence of local solubility of hydrophobic molecules in the liquid-vapor interface of water". *Journal of Chemical Physics* 141.18 (Nov. 2014), p. 18C516. DOI: 10.1063/1.4896236.

[17] A. Haji-Akbari, R. S. DeFever, S. Sarupria, and P. G. Debenedetti. "Suppression of sub-surface freezing in free-standing thin films of a coarse-grained model of water". *Physical Chemistry Chemical Physics* 16.47 (Nov. 2014), pp. 25916–25927. DOI: 10.1039/c4cp03948c.

[18] A. Haji-Akbari and P. G. Debenedetti. "Computational investigation of surface freezing in a molecular model of water". *Proceedings of the National Academy of Sciences* 114.13 (Mar. 2017), pp. 3316–3321. DOI: 10.1073/PNAS.1620999114.

[19] S. M. Malek, P. H. Poole, and I. Saika-Voivod. "Surface tension of supercooled water nanodroplets from computer simulations". *Journal of Chemical Physics* 150.23 (June 2019), p. 234507. DOI: 10.1063/1.5096990. arXiv: 1905.13709.

[20] D. Eisenberg and W. Kauzmann. *The Structure and Properties of Water*. Oxford University Press, 2005. ISBN: 0-19-857026-0,9780198570264.

[21] E. Brini, C. J. Fennell, M. Fernandez-Serra, B. Hribar-Lee, M. Lukšič, et al. "How Water's Properties Are Encoded in Its Molecular Structure and Energies". *Chemical Reviews* 117.19 (Oct. 2017), pp. 12385–12414. DOI: 10.1021/acs.chemrev.7b00259.

[22] P. G. Debenedetti. "Supercooled and glassy water". *Journal of Physics: Condensed Matter* 15.45 (Nov. 2003), R1669–R1726. DOI: 10.1088/0953-8984/15/45/R01.

[23] P. H. Handle, T. Loerting, and F. Sciortino. *Supercooled and glassywater:Metastable liquid(s), amorphous solid(s), and a no-man's land*. Dec. 2017. DOI: 10.1073/pnas.1700103114.

[24] R. Ludwig and D. Paschek. "Wasser: Anomalien und Rätsel". *Chemie in unserer Zeit* 39.3 (June 2005), pp. 164–175. DOI: 10.1002/ciuz.200400341.

[25] C. A. Angell. "Supercooled Water". *Annual Review of Physical Chemistry* 34.1 (Oct. 1983), pp. 593–630. DOI: 10.1146/annurev.pc.34.100183.003113.

[26] P. G. Debenedetti. *Metastable liquids : concepts and principles*. Princeton University Press, 1996, p. 411. ISBN: 9780691085951.

[27] O. Mishima and H. E. Stanley. *The relationship between liquid, supercooled and glassy water*. Nov. 1998. DOI: 10.1038/24540.

[28] I. Kohl, L. Bachmann, A. Hallbrucker, E. Mayer, and T. Loerting. "Liquid-like relaxation in hyperquenched water at $\leq$ 140 K". *Physical Chemistry Chemical Physics* 7.17 (Sept. 2005), pp. 3210–3220. DOI: 10.1039/b507651j.

[29] P. G. Debenedetti and H. E. Stanley. "Supercooled and glassy water". *Physics Today* 56.6 (2003), pp. 40–46. DOI: 10.1063/1.1595053.

[30] P. H. Poole, F. Sciortino, U. Essmann, and H. E. Stanley. "Phase behaviour of metastable water". *Nature* 360.6402 (1992), pp. 324–328. DOI: 10.1038/360324a0.

[31] S. Aasland and P. F. McMillan. "Density-driven liquid-liquid phase separation in the system AI_2O_3–Y_2O_3". *Nature* 369.6482 (1994), pp. 633–636. DOI: 10.1038/369633a0.

[32] A. Cadien, Q. Y. Hu, Y. Meng, Y. Q. Cheng, M. W. Chen, et al. "First-order liquid-liquid phase transition in cerium". *Physical Review Letters* 110.12 (Mar. 2013), p. 125503. DOI: 10.1103/PhysRevLett.110.125503.

[33] N. Goldenfeld. *Lectures On Phase Transitions And The Renormalization Group*. Westview Press, 1992.

[34] J. Russo and H. Tanaka. "Understanding water's anomalies with locally favoured structures". *Nature Communications* 5.1 (Apr. 2014), pp. 1–11. DOI: 10.1038/ncomms4556. arXiv: 1308.4231.

[35] J. L. Abascal and C. Vega. "Widom line and the liquid-liquid critical point for the TIP4P/2005 water model". *Journal of Chemical Physics* 133.23 (Dec. 2010), p. 234502. DOI: 10.1063/1.3506860.

[36] G. Pallares, M. E. M. Azouzi, M. A. González, J. L. Aragones, J. L. F. Abascal, et al. "Anomalies in bulk supercooled water at negative pressure". *Proceedings of the National Academy of Sciences* 111.22 (June 2014), pp. 7936–7941. DOI: 10.1073/PNAS.1323366111.

[37] W. C. Röntgen. "Ueber die Constitution des flüssigen Wassers". *Annalen der Physik* 281.1 (Jan. 1892), pp. 91–97. DOI: 10.1002/andp.18922810108.

[38] V. Holten, J. V. Sengers, and M. A. Anisimov. "Equation of State for Supercooled Water at Pressures up to 400 MPa". *Journal of Physical and Chemical Reference Data* 43.4 (Oct. 2014), p. 1021. DOI: 10.1063/1.4895593. arXiv: 1403.6777.

[39] H. Tanaka. "Importance of many-body orientational correlations in the physical description of liquids". *Faraday Discussions* 167.0 (Dec. 2013), pp. 9–76. DOI: 10.1039/c3fd00110e.

[40] J. A. Sellberg, C. Huang, T. A. McQueen, N. D. Loh, H. Laksmono, et al. "Ultrafast X-ray probing of water structure below the homogeneous ice nucleation temperature". *Nature* 510.7505 (June 2014), pp. 381–384. DOI: 10.1038/nature13266.

[41] K. Amann-Winkel, C. Gainaru, P. H. Handle, M. Seidl, H. Nelson, et al. "Water's second glass transition". *Proceedings of the National Academy of Sciences of the United States of America* 110.44 (Oct. 2013), pp. 17720–17725. DOI: 10.1073/pnas.1311718110.

[42] F. Perakis, K. Amann-Winkel, F. Lehmköhler, M. Sprung, D. Mariedahl, et al. *Diffusive dynamics during the high-To-low density transition in amorphous ice*. Aug. 2017. DOI: 10.1073/pnas.1705303114.

[43] M. V. Berry. "The molecular mechanism of surface tension". *Physics Education* 6.2 (1971), p. 79. DOI: 10.1088/0031-9120/6/2/001.

[44] J. Pellicer, V. García-Morales, L. Guanter, M. J. Hernández, and M. Dolz. "On the experimental values of the water surface tension used in some textbooks". *American Journal of Physics* 70.7 (July 2002), pp. 705–709. DOI: 10.1119/1.1477431.

[45] A. Marchand, J. H. Weijs, J. H. Snoeijer, and B. Andreotti. "Why is surface tension a force parallel to the interface?" *American Journal of Physics* 79.10 (Oct. 2011), pp. 999–1008. DOI: 10.1119/1.3619866. arXiv: 1211.3854.

[46] J. Speight. *Lange's Handbook of Chemistry, 70th Anniversary Edition*. McGraw-Hill Companies,Incorporated, 2004. ISBN: 0071432205.

[47] J. G. Kirkwood and F. P. Buff. "The statistical mechanical theory of surface tension". *The Journal of Chemical Physics* 17.3 (Mar. 1949), pp. 338–343. DOI: 10.1063/1.1747248.

[48] J. Alejandre, D. J. Tildesley, and G. A. Chapela. "Molecular dynamics simulation of the orthobaric densities and surface tension of water". *The Journal of Chemical Physics* 102.11 (Mar. 1995), pp. 4574–4583. DOI: 10.1063/1.469505.

[49] R. C. Tolman. "Consideration of the Gibbs theory of surface tension". *The Journal of Chemical Physics* 16.8 (Aug. 1948), pp. 758–774. DOI: 10.1063/1.1746994.

[50] IAPWS. *Revised Release on Surface Tension of Ordinary Water Substance*. Tech. rep. Moscow, Russia, 2014.

[51] N. B. Vargaftik, B. N. Volkov, and L. D. Voljak. "International Tables of the Surface Tension of Water". *Journal of Physical and Chemical Reference Data* 12.3 (July 1983), pp. 817–820. DOI: 10.1063/1.555688.

[52] M. Sega, G. Horvai, and P. Jedlovszky. "Microscopic Origin of the Surface Tension Anomaly of Water". *Langmuir* 30.11 (Mar. 2014), pp. 2969–2972. DOI: 10.1021/la404868e.

[53] P. T. Hacker. *Experimental Values of the Surface Tension of Supercooled Water*. Tech. rep. National Advisory Committee for Aeronautics. Lewis Flight Propulsion Lab., Oct. 1951.

[54] M. A. Floriano and C. A. Angell. "Surface tension and molar surface free energy and entropy of water to -27.2 °C". *Journal of Physical Chemistry®* 94.10 (1990), pp. 4199–4202. DOI: 10.1021/j100373a059.

[55] E. H. Trinh and K. Ohsaka. "Measurement of density, sound velocity, surface tension, and viscosity of freely suspended supercooled liquids". *International Journal of Thermophysics* 16.2 (Mar. 1995), pp. 545–555. DOI: 10.1007/BF01441920.

[56] J. Hrubý, V. Vinš, R. Mareš, J. Hykl, and J. Kalová. "Surface tension of supercooled water: No inflection point down to -25 °c". *Journal of Physical Chemistry Letters* 5.3 (Feb. 2014), pp. 425–428. DOI: 10.1021/jz402571a.

[57] V. Vinš, M. Fransen, J. Hykl, and J. Hrubý. "Surface Tension of Supercooled Water Determined by Using a Counterpressure Capillary Rise Method". *Journal of Physical Chemistry B* 119.17 (Apr. 2015), pp. 5567–5575. DOI: 10.1021/acs.jpcb.5b00545.

[58] V. Vinš, J. Hošek, J. Hykl, and J. Hrubý. "Surface Tension of Supercooled Water: Inflection Point-Free Course down to 250 K Confirmed Using a Horizontal Capillary Tube". *Journal of Chemical and Engineering Data* 62.11 (Nov. 2017), pp. 3823–3832. DOI: 10.1021/acs.jced.7b00519.

[59] C. Rowley. *Simulated Radial Distribution Functions for Solid, Liquid, and Gaseous Argon.svg - Wikimedia Commons*. URL: https://en.wikibooks.org/wiki/Molecular_Simulation/Radial_Distribution_Functions (visited on 09/09/2020).

[60] M. P. Allen and D. J. Tildesley. *Computer Simulation of Liquids*. Oxford University Press, 2017. ISBN: 9780198803195.

[61] J. P. Hansen and I. R. McDonald. *Theory of Simple Liquids: with Applications to Soft Matter*. Elsevier Science, 2013. ISBN: 9780123870339.

[62] M. J. Louwerse and E. J. Baerends. "Calculation of pressure in case of periodic boundary conditions". *Chemical Physics Letters* 421.1-3 (Apr. 2006), pp. 138–141. DOI: 10.1016/j.cplett.2006.01.087.

[63] Lindahl, Abraham, Hess, and van der Spoel. *GROMACS 2019.3 Source code*. June 2019. DOI: 10.5281/ZENODO.3243833.

[64] Lindahl, Abraham, Hess, and van der Spoel. "GROMACS 2019.3 Manual" (June 2019). DOI: 10.5281/ZENODO.3243834.

[65] S. Nosé. "A unified formulation of the constant temperature molecular dynamics methods". *The Journal of Chemical Physics* 81.1 (July 1984), pp. 511–519. DOI: 10.1063/1.447334.

[66] W. G. Hoover. "Canonical dynamics: Equilibrium phase-space distributions". *Physical Review A* 31.3 (Mar. 1985), pp. 1695–1697. DOI: 10.1103/PhysRevA.31.1695.

[67] M. Rao and D. Levesque. "Surface structure of a liquid film". *The Journal of Chemical Physics* 65.8 (Oct. 1976), pp. 3233–3236. DOI: 10.1063/1.433495.

[68] A. Ben-Naim. “Statistical mechanics of ”waterlike ” particles in two dimensions. I. Physical model and application of the Perçus-Yevick equation”. *The Journal of Chemical Physics* 54.9 (May 1971), pp. 3682–3695. DOI: 10.1063/1.1675414.

[69] B. Hess. “P-LINCS: A parallel linear constraint solver for molecular simulation”. *Journal of Chemical Theory and Computation* 4.1 (Jan. 2008), pp. 116–122. DOI: 10.1021/ct700200b.

[70] J. A. Barker and R. O. Watts. “Structure of water; A Monte Carlo calculation”. *Chemical Physics Letters* 3.3 (Mar. 1969), pp. 144–145. DOI: 10.1016/0009-2614(69)80119-3.

[71] A. Rahman and F. H. Stillinger. “Molecular Dynamics Study of Liquid Water”. *The Journal of Chemical Physics* 55.7 (Oct. 1971), pp. 3336–3359. DOI: 10.1063/1.1676585.

[72] H. J. C. Berendsen, J. P. M. Postma, W. F. van Gunsteren, and J. Hermans. “Interaction Models for Water in Relation to Protein Hydration”. *Intermolecular Forces*. Springer, Dordrecht, 1981, pp. 331–342. DOI: 10.1007/978-94-015-7658-1_21.

[73] H. J. C. Berendsen, J. R. Grigera, and T. P. Straatsma. “The missing term in effective pair potentials”. *Journal of Physical Chemistry* 91.24 (1987), pp. 6269–6271. DOI: 10.1021/j100308a038.

[74] W. L. Jorgensen. “Transferable Intermolecular Potential Functions. Application to Liquid Methanol Including Internal Rotation”. *Journal of the American Chemical Society* 103.2 (1981), pp. 341–345. DOI: 10.1021/ja00392a017.

[75] W. L. Jorgensen, J. Chandrasekhar, J. D. Madura, R. W. Impey, and M. L. Klein. “Comparison of simple potential functions for simulating liquid water”. *The Journal of Chemical Physics* 79.2 (July 1983), pp. 926–935. DOI: 10.1063/1.445869.

[76] M. W. Mahoney and W. L. Jorgensen. “A five-site model for liquid water and the reproduction of the density anomaly by rigid, nonpolarizable potential functions”. *Journal of Chemical Physics* 112.20 (May 2000), pp. 8910–8922. DOI: 10.1063/1.481505.

[77] C. L. Zhao, D. X. Zhao, C. C. Bei, X. N. Meng, S. Li, et al. “Seven-Site Effective Pair Potential for Simulating Liquid Water”. *Journal of Physical Chemistry B* 123.21 (May 2019), pp. 4594–4603. DOI: 10.1021/acs.jpcb.9b03149.

[78] H. J. C. Berendsen, J. R. Grigera, and T. P. Straatsma. “The missing term in effective pair potentials”. *Journal of Physical Chemistry* 91.24 (1987). DOI: 10.1021/j100308a038.

[79] J. L. Abascal and C. Vega. “A general purpose model for the condensed phases of water: TIP4P/2005”. *Journal of Chemical Physics* 123.23 (Dec. 2005), p. 234505. DOI: 10.1063/1.2121687.

[80] I. Shvab and R. J. Sadus. "Atomistic water models: Aqueous thermodynamic properties from ambient to supercritical conditions". *Fluid Phase Equilibria* 407 (May 2015), pp. 7–30. DOI: 10.1016/j.fluid.2015.07.040.

[81] R. Sakamaki, A. K. Sum, T. Narumi, and K. Yasuoka. "Molecular dynamics simulations of vapor/liquid coexistence using the nonpolarizable water models". *Journal of Chemical Physics* 134.12 (Mar. 2011), p. 124708. DOI: 10.1063/1.3574038.

[82] S. Harrington, P. H. Poole, F. Sciortino, and H. E. Stanley. "Equation of state of supercooled water simulated using the extended simple point charge intermolecular potential". *Journal of Chemical Physics* 107.18 (Nov. 1997), pp. 7443–7450. DOI: 10.1063/1.474982.

[83] F. Sciortino, E. La Nave, and P. Tartaglia. "Physics of the liquid-liquid critical point". *Physical Review Letters* 91.15 (Oct. 2003), p. 155701. DOI: 10.1103/PhysRevLett.91.155701.

[84] D. T. Limmer and D. Chandler. "Theory of amorphous ices". *Proceedings of the National Academy of Sciences of the United States of America* 111.26 (July 2014), pp. 9413–9418. DOI: 10.1073/pnas.1407277111. arXiv: 1306.4728.

[85] F. Bresme, J. W. Biddle, J. V. Sengers, and M. A. Anisimov. "Communication: Minimum in the thermal conductivity of supercooled water: A computer simulation study". *Journal of Chemical Physics* 140.16 (Apr. 2014), p. 161104. DOI: 10.1063/1.4873167.

[86] C. McBride. *SklogWiki*. URL: http://www.sklogwiki.org/SklogWiki/index.php/SPC/E_model_of_water (visited on 06/18/2020).

[87] M. J. Abraham, T. Murtola, R. Schulz, S. Páll, J. C. Smith, et al. "Gromacs: High performance molecular simulations through multi-level parallelism from laptops to supercomputers". *SoftwareX* 1-2 (Sept. 2015), pp. 19–25. DOI: 10.1016/j.softx.2015.06.001.

[88] M. Sega, G. Hantal, B. Fábián, and P. Jedlovszky. "Pytim: A python package for the interfacial analysis of molecular simulations". *Journal of Computational Chemistry* 39.25 (Sept. 2018), pp. 2118–2125. DOI: 10.1002/jcc.25384.

[89] N. Michaud-Agrawal, E. J. Denning, T. B. Woolf, and O. Beckstein. "MDAnalysis: A toolkit for the analysis of molecular dynamics simulations". *Journal of Computational Chemistry* 32.10 (July 2011), pp. 2319–2327. DOI: 10.1002/jcc.21787.

[90] R. Gowers, M. Linke, J. Barnoud, T. Reddy, M. Melo, et al. "MDAnalysis: A Python Package for the Rapid Analysis of Molecular Dynamics Simulations". *Proceedings of the 15th Python in Science Conference*. SciPy, 2016, pp. 98–105. DOI: 10.25080/majora-629e541a-00e.

[91] L. B. Pártay, G. Hantal, P. Jedlovszky, Á. Vincze, and G. Horvai. "A new method for determining the interfacial molecules and characterizing the surface roughness in computer simulations. Application to the liquid–vapor interface of water". *Journal of Computational Chemistry* 29.6 (Apr. 2008), pp. 945–956. DOI: 10.1002/jcc.20852.

[92] M. Sega, S. S. Kantorovich, P. Jedlovszky, and M. Jorge. "The generalized identification of truly interfacial molecules (ITIM) algorithm for nonplanar interfaces". *Journal of Chemical Physics* 138.4 (Jan. 2013), p. 044110. DOI: 10.1063/1.4776196.

[93] M. J. Cuthbertson and P. H. Poole. "Mixturelike behavior near a liquid-liquid phase transition in simulations of supercooled water". *Physical Review Letters* 106.11 (Mar. 2011), p. 115706. DOI: 10.1103/PhysRevLett.106.115706. arXiv: 1102.5256.

[94] F. H. Stillinger. "Rigorous basis of the Frenkel-Band theory of association equilibrium". *The Journal of Chemical Physics* 38.7 (Apr. 1963), pp. 1486–1494. DOI: 10.1063/1.1776907.

[95] M. Tanemura, Y. Hiwatari, H. Matsuda, T. Ogawa, N. Ogita, et al. "Geometrical Analysis of Crystallization of the Soft-Core Model". *Progress of Theoretical Physics* 58.4 (Oct. 1977), pp. 1079–1095. DOI: 10.1143/ptp.58.1079.

[96] P. R. Ten Wolde and D. Frenkel. "Computer simulation study of gas-liquid nucleation in a Lennard-Jones system". *Journal of Chemical Physics* 109.22 (Dec. 1998), pp. 9901–9918. DOI: 10.1063/1.477658.

[97] J. Losey and R. J. Sadus. "Structural behavior of fluids from the vapor and liquid region to the supercritical phase". *Physical Review E* 100.5 (Nov. 2019). DOI: 10.1103/PhysRevE.100.052132.

[98] E. Duboué-Dijon and D. Laage. "Characterization of the Local Structure in Liquid Water by Various Order Parameters". *The Journal of Physical Chemistry B* 119.26 (July 2015), pp. 8406–8418. DOI: 10.1021/acs.jpcb.5b02936.

[99] S. M. Malek, P. H. Poole, and I. Saika-Voivod. "Thermodynamic and structural anomalies of water nanodroplets". *Nature Communications* 9.1 (Dec. 2018), pp. 1–9. DOI: 10.1038/s41467-018-04816-2.

[100] J. G. Eberhart. "The Surface Tension of Binary Liquid Mixtures". *The Journal of Physical Chemistry* 70.4 (Apr. 1966), pp. 1183–1186. DOI: 10.1021/j100876a035.